Acceptorless amine dehydrogenation and transamination using Pd-doped layered double hydroxides

Diana Ainembabazi, Nan An, Jinesh Manayil, Kare Wilson, Adam Lee, Adelina Voutchkova-Kostal

The synthesis, characterization, and activity of Pd-doped layered double hydroxides (Pd-LDHs) for for acceptorless amine dehydrogenation is reported. These multifunctional catalysts comprise Brønsted basic and Lewis acidic surface sites that stabilize Pd species in 0, 2+, and 4+ oxidation states. Pd speciation and corresponding catalytic performance is a strong function of metal loading. Excellent activity is observed for the oxidative transamination of primary amines and acceptorless dehydrogenation of secondary amines to secondary imines using a low Pd loading (0.5 mol%), without the need for oxidants. N-heterocycles, such as indoline, 1,2,3,4-tetrahydroquinoline, and piperidine, are dehydrogenated to the corresponding aromatics with high yields. The relative yields of secondary imines are proportional to the calculated free energy of reaction, while yields for oxidative amination correlate with the electrophilicity of primary imine intermediates. Reversible amine dehydrogenation and imine hydrogenation determine the relative imine:amine selectivity. Poisoning tests evidence that Pd-LDHs operate heterogeneously, with negligible metal leaching; catalysts can be regenerated by acid dissolution and re-precipitation.

File list (2)

ESI_Aug22.pdf (9.40 MiB)	view on ChemRxiv • download file
Dehydrog_imine_GC_clean_archive_no template.pdf (3.97 MiB)	view on ChemRxiv • download file

Electronic Supporing Information for
Acceptorless Amine Dehydrogenation with Pd-doped Layered Double Hydroxides

Diana Ainembabazi, Nan An, Jinesh, C. Manayil, Karen Wilson, Adam F. Lee and Adelina
M. Voutchkova-Kostal

Chemistry Department, George Washington University, 800 22nd Street NW,

Washington, D. C. 20052

Avoutchkova@gwu.edu

1. Experimental procedure for flow synthesis of LDHs.

Solution **A** was prepared by mixing Mg(NO$_3$)$_2$·6H$_2$O, Al(NO$_3$)$_3$·9H$_2$O and Pd(NO$_3$)$_2$ dissolved in total 70 mL of DI water (Table S1). Solution **B** was prepared using a mixture of NaOH (0.040 mol) and Na$_2$CO$_3$ (0.0025 mol) dissolved into 70 mL of DI water. Two 60-mL plastic syringes were filled with solutions **A** and **B** respectively and placed on a syringe pump connected to 5-mm diameter polyethylene tubing jointed using a Y connector (Figure S1). The syringe pump was set with a flow rate of 4 mL/min and was positioned to drip into a beaker containing 100 mL of DI water. The mixture in the beaker was stirred at 200 rpm at 65 °C for 2 h. After that time the mixture was cooled at room temperature, filtered and washed with DI water until the pH of the filtrate was neutral. The resulting LDHs were dried at 110°C for 12 hours.

Table S-1. Molar concentrations (mM) of metal salts in solution A for flow synthesis of Pd-LDH and Mg-Al LDH.

Sample	mM of metal salts in solution A		
	Mg^{2+}	Al^{3+}	Pd^{2+}
0.1% Pd-LDH	214.0	71.4	0.29
0.5% Pd-LDH	212.9	71.4	1.43
5% Pd-LDH	200.0	71.4	14.3
Mg:Al LDH	214.3	71.4	-

B: Bases including NaOH and NaCO$_3$

A: Salts (Pd^{2+}, Al^{3+} and Mg^{2+} aqueous solution)

Water
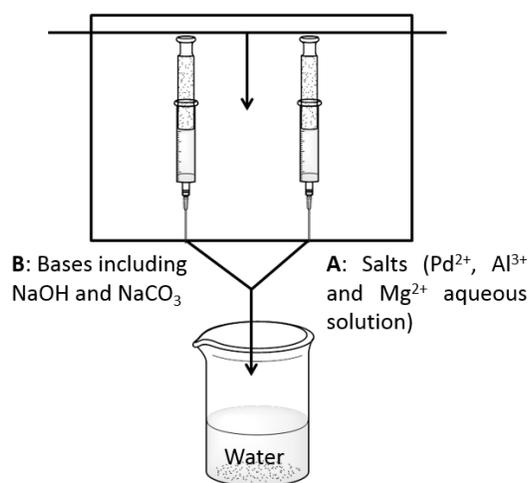
Figure S-1. Schematic diagram of the continuous flow apparatus for synthesis of Pd-LDH

2. Characterization

Elemental analysis was carried out with inductively coupled plasma atomic emission spectroscopy (ICP-AES) on a Shimadzu ICPE-9820 Plasma Atomic Emission Spectrometer. Powder X-Ray Diffraction (PXRD) patterns were obtained using a Rigaku MiniFlex II X-Ray defractometer.

Thermogravometric analysis (TGA) was performed on a Perkin Elmer Pyris 1 TGA. Samples were heated from 30-650 °C at 20 °C min^{-1} in nitrogen.

X-ray Photoelectron Spectroscopy was performed on a Kratos AXIS 165 Photoelectron Spectrometer. XPS data is collected both using Mg Kα (1253.6 eV) anode and Monochromatic Al (1486.7 eV) X-ray sources at 240W. Charge neutralization was carried out to minimize surface charging. Hydrocarbon C 1s binding energies were referenced at 284.8eV. Pd 3d binding energies were confirmed by Mg anode due to the overlapping of Magnesium Auger Electron peaks (Mg KLL) with Pd 3d signals when Al anode was used. Binding energies of other elements are confirmed using the monochromatic Al X-ray source.

Transmission Electron Microscope (TEM) images were collected on Talos F200X under 200kV FEG with Ceta 16M camera. Fast Energy-dispersive X-ray spectroscopy (EDS) mapping was carried out using the built-in Silicon Drift Detector (Super-X EDS Detector).

Nitrogen isotherms were measure on a Micrometric TriStar surface analyzer at liquid nitrogen temperatures. Samples were degassed under vacuum at 150 ^{o}C for 3 hours prior to measurement. Surface area was calculated using the BET method, pore size and volumes were calculated via the BJH method on the desorption isotherm.

The acid-base properties of the catalysts were studied by temperature-programmed desorption of CO2 and propylamine, measured on a Quantochrome ChemBET system coupled to an MKS Minilab QMS. The samples were degassed at 150 ^{o}C for 3h, then saturated with CO_2 at room temperature for XXX hours. Desorption profiles of chemisorbed CO2 were obtained by heating the sample to 800 ^{o}C under He. The quantity of CO_2 adsorbed was determined by CO_2 pulse titration at 40 ^{o}C.

For propylamine – difference in conditions? How is the sample saturated with propylamine? … the total quantity of propylamine adsorbed was determined by integrating the total desorption peak area of amu 41, corresponding to propene.

NMR spectra were recorded on an Agilent 400 MHz spectrometer.

GC-FID chromatograms were recorded on an Agilent 6890N GC System using a column with a DB-5 stationary phase.

(a)
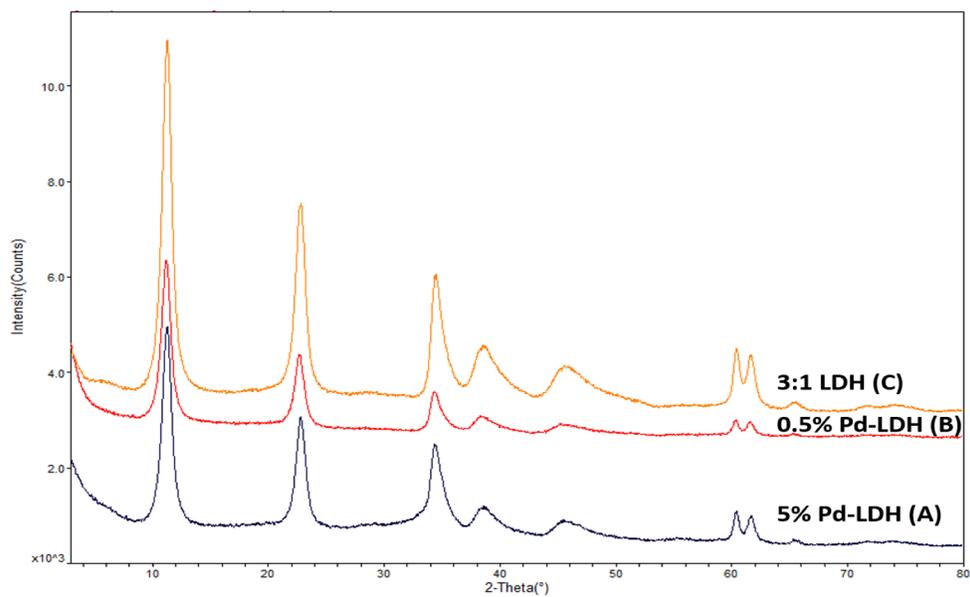
(b)
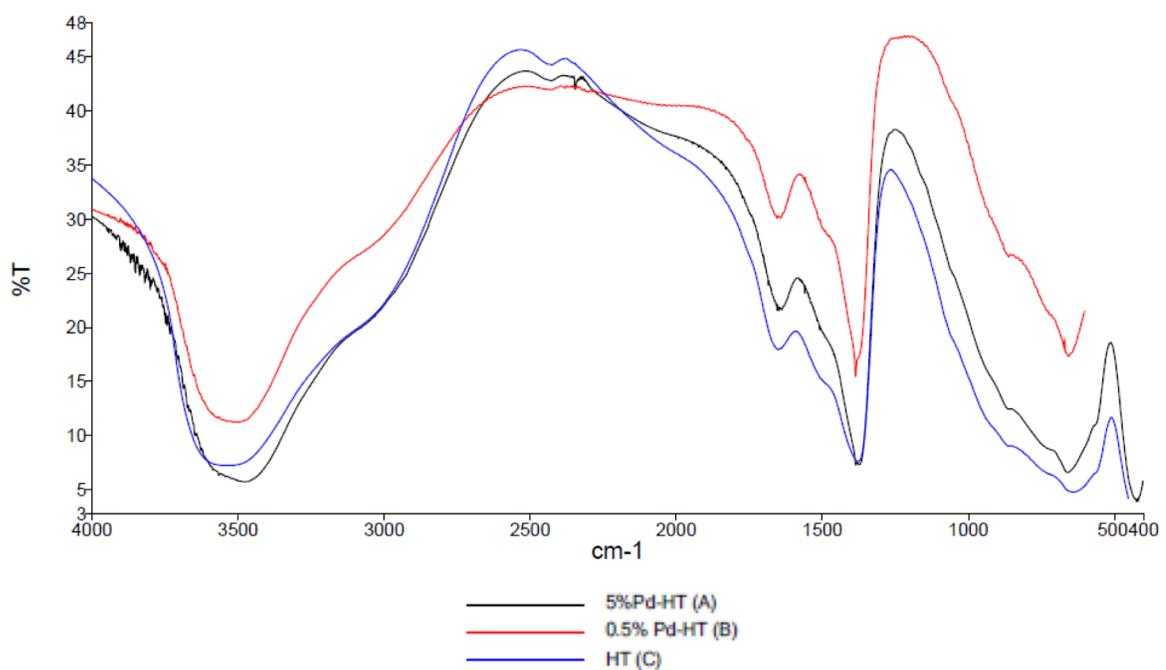
Figure S-2. (a) PXRD patterns and (b) FTIR of Pd-LDH catalysts and Mg-Al LDH.

Table S-2. Characterization data of Pd-LDHs and control Mg-Al LDH (HT)*:* elemental composition and PXRD crystallographic parameters (*a, c and L*).

| Catalyst	Elemental composition (RSD), metal mol %[1]				Crystallographic parameters		
	Pd^{2+}	Mg^{2+}	Al^{3+}	M^{2+}/M^{3+}	a (Å)*	c (Å)*	L (nm)
5% Pd-LDH (*A*)	4.53 (0.40)	70.5 (0.60)	24.8 (0.10)	2.98	3.052	23.07	10.4
0.5% Pd-LDH (*B*)	0.54 (0.81)	73.9 (0.63)	25.7 (0.65)	2.90	3.058	23.56	10.3
Mg-Al LDH (HT) (*C*)	-	75.6 (0.23)	24.4 (0.23)	3.09	3.066	23.35	10.8

[1]Mol% calculated as fraction of all metals present (Mg, Al, Pd); **a*, the average cation-cation distance; **c*, three times the distance from the center of one brucite-like layer to the next layer; *L*, the average crystallite size (calculated using Scherrer's formula).[1]

Table S-3. BET surface area, pore diameter, pore volume, basicity and acidity of Pd-LDHs and Mg-Al LDH (catalysts *A* -*C*).

Catalyst	BET Surface area, m^2/g	Pore diameter, Å	Total pore volume, cm^3/g	Micropore volume	Basicity[a] mmol/g	Acidity[b] mmol/g
5% Pd-LDH (*A*)	52.8	66.1	0.132	0.0021	0.03	0.87
0.5% Pd-LDH (*B*)	102.6	41.3	0.143	0.0041	0.06	0.52
Mg-Al LDH (HT) (*C*)	148.0	36.0	0.260	0.0048	0.10	0.14

[a]Propyl amine temperature-programmed desorption ; [b]CO_2 pulse titration;

Table S-4 Binding energies and peak positions for 5%Pd-LDH (**A**) and 0.5%Pd-LDH (**B**) as observed by XPS.

Species	Atomic Orbitals	5%Pd-LDH	0.5%Pd-LDH	Reference BE (eV)
Pd^0	$3d_{3/2}$ (eV)	340.6	-	340.4[2]
	$3d_{5/2}$ (eV)	335.3	-	335.1[2]
Pd^{2+}	$3d_{3/2}$ (eV)	341.6	341.6	341.6[3]
	$3d_{5/2}$ (eV)	336.3	336.3	336.3[3]
Pd^{4+}	$3d_{3/2}$ (eV)	343.4	343.4	343.0[3]
	$3d_{5/2}$ (eV)	338.2	338.2	337.9[3]
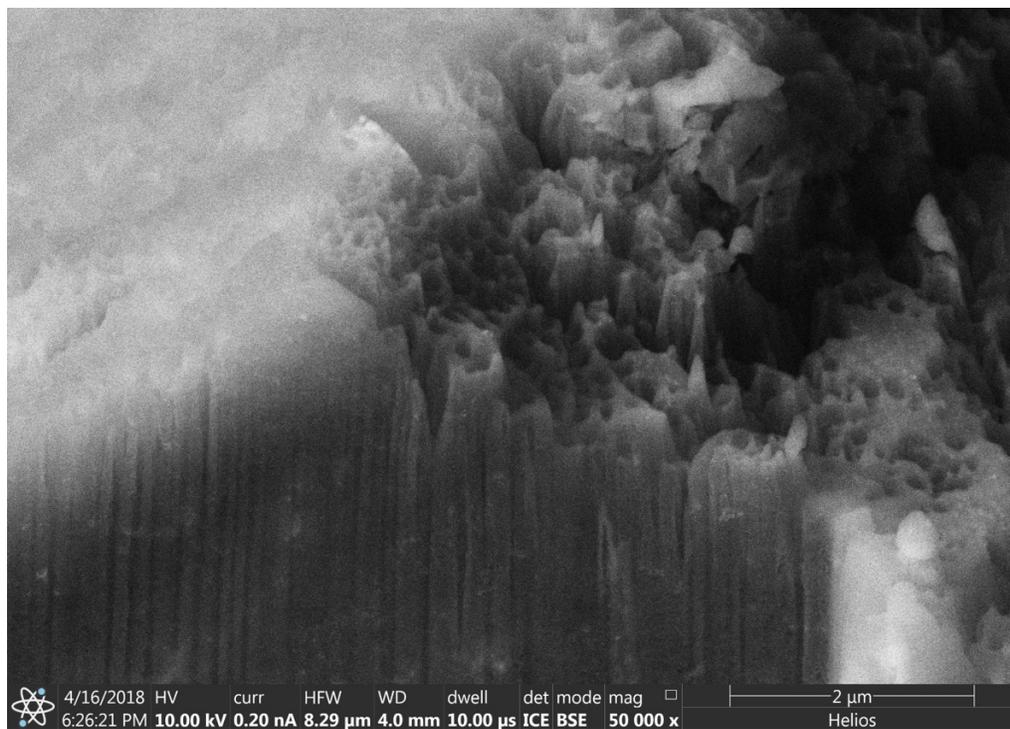
Figure S-3. SEM image of a FIB-etched region of 5%Pd-LDH (**A**) (2 μm scale), showing channel-like pores.
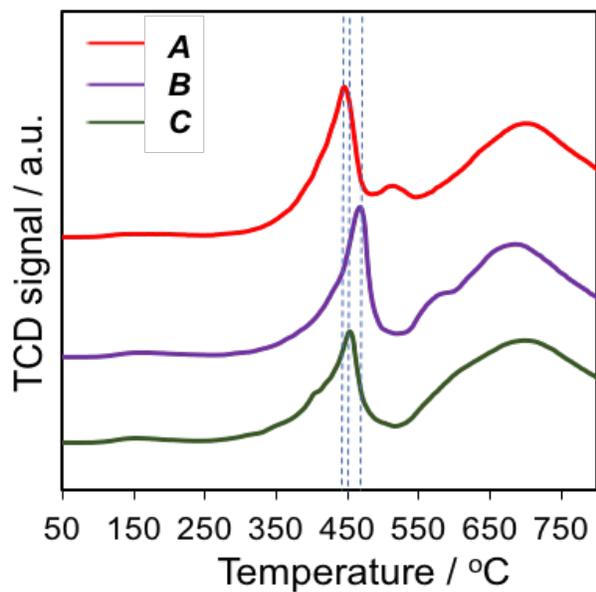
Figure S4. Temperature programmed desorption of CO_2 for catalysts *A*, *B* and *C*.
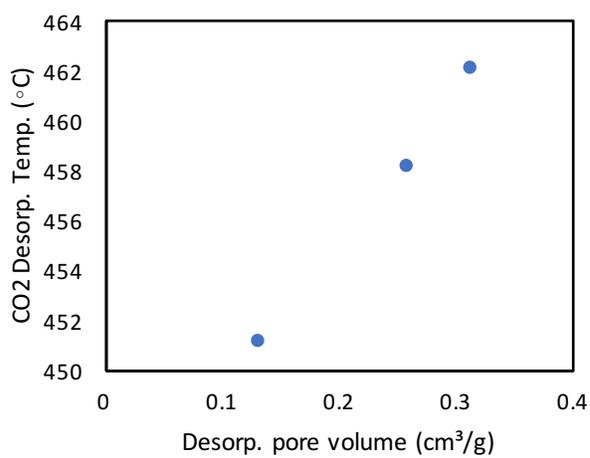
Figure S5. N_2 desorption pore volume versus temperature of CO_2 desorption feature at ~ 450°C from temperature programmed desorption of catalysts *A*, *B* and *C.*

(a)

(b)
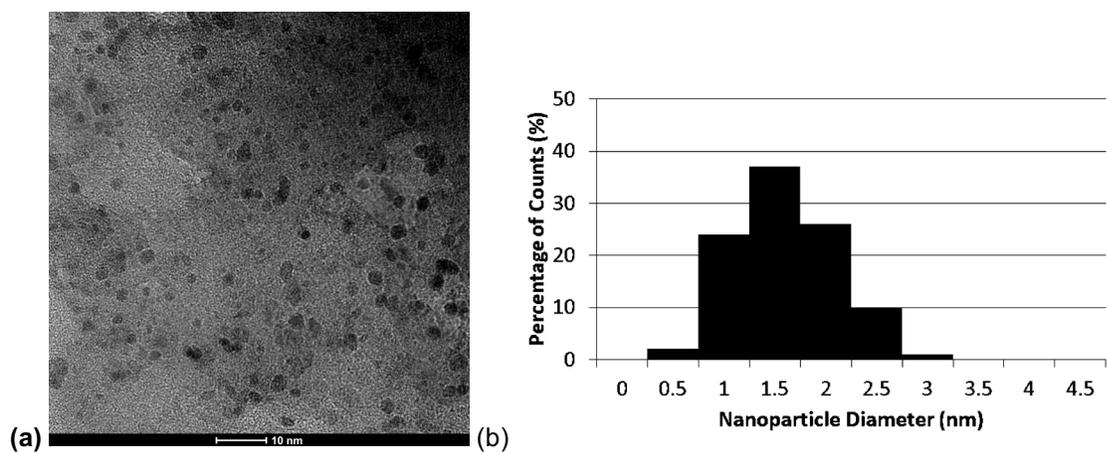
Figure S-6 (a) TEM image of 5%Pd-LDH (*A*) (10 nm scale); (b) Distribution of nanoparticle sizes of 5%Pd-LDH based on sampling of 500 particles.
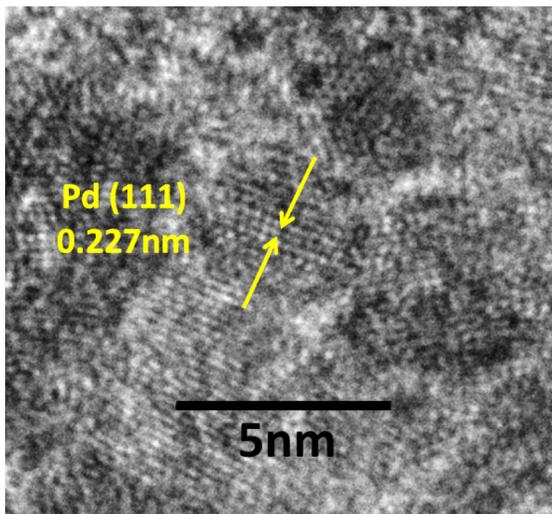
(a)
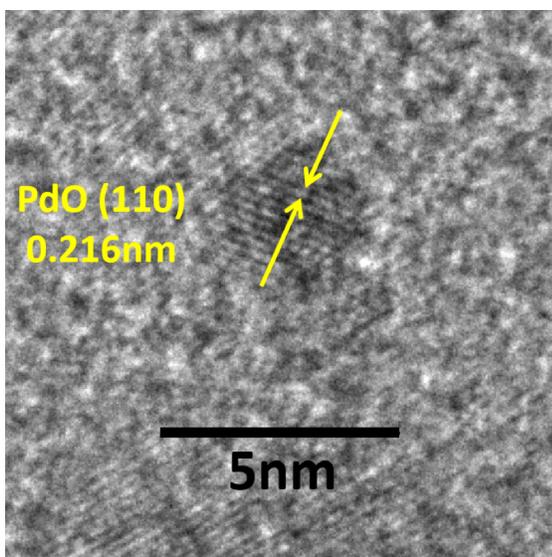
(b)

Figure S-7. HRTEM and crystal lattice of 5%Pd-LDH (*A*) showing (a) Pd (111) and (b) Pd (110) phases.
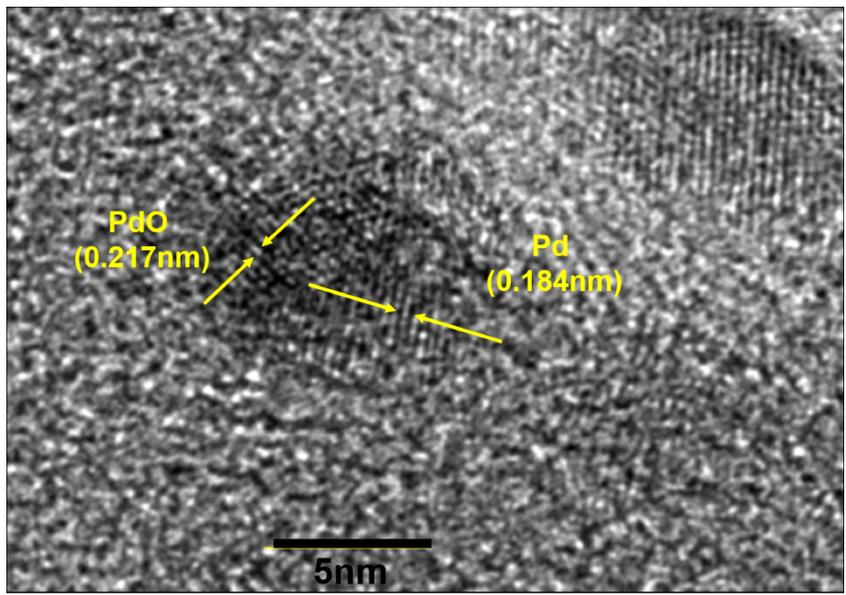
(a)
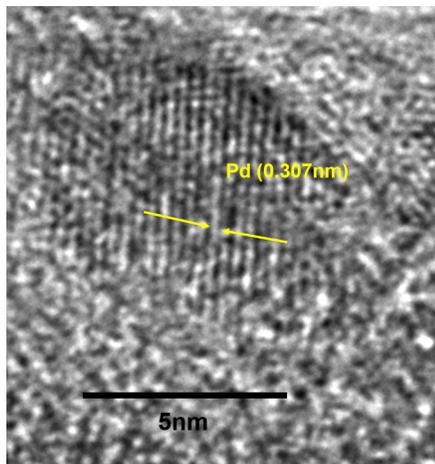
(b)

Figure S-8. (a & b) HRTEM and crystal lattice of 5%Pd/C showing different phases of Pd.

Table S-5. Free energy (ΔG_{rxn}) for dehydrogenation of secondary amines calculated using DFT's B3LYP method with 6-31G(d) basis set at 423K with toluene as the implicit solvent.
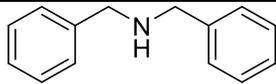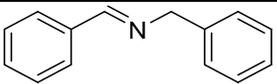
| Entry	Substrate	Product	ΔG_{rxn}, kJ/mole	ΔG_f[Imine] x10^6, kJ/mole
1			6.89	-1.56
2			10.01	-1.46
3			2.92	-9.58
4			40.40	-9.58
5			13.79	-9.71
6			0.50	-0.65
7			-6.79	-1.06
8			-11.29	-0.96
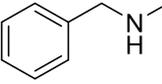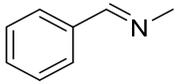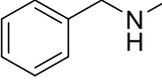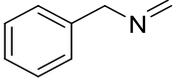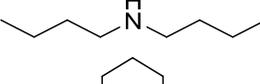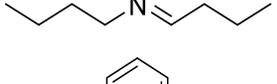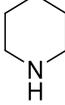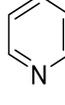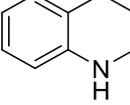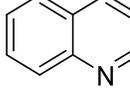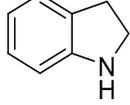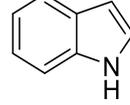
Table S-6. Substrate scope for dehydrogenative coupling of primary amine under microwave heating.
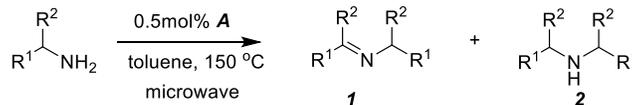
entry	R^1	R^2	yields		conv.	time/hr
			1	2		
1	Ph	H	94	3	99	3
2	Ph	Me	75	19	96	6
3	Ph(p-OMe)	H	80	20	99	3
4	Ph(p-F)	H	87	3	95	3
5	hexyl	H	42	31	74	8
6	Ph(CH$_2$)	H	0	30	59	8

Conditions: substrate (1 mmol), cat *A* (0.005 mol Pd, 10.0 mg), toluene (1 mL), microwave heating at 150 °C; yields determined using an internal standard by NMR and GC-FID.

Table S-7. Free energy (ΔG_{rxn}) for dehydrogenative amine coupling calculated using DFT's B3LYP method with 6-31G(d) basis set at 423K with toluene as the implicit solvent.
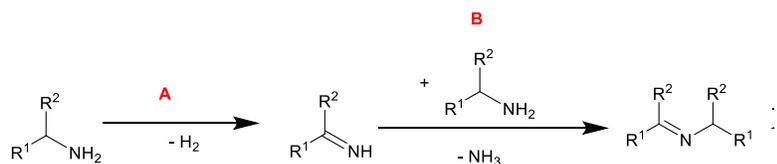
| Entry	Substrate	Product	ΔG_{rxn} (steps A + B) kJ/mole
1			-4.96
2			34.60
3			22.48
4			-1.51
5			5.08
6			12.09
7			3.16
8			37.18

Table S-8. Electrophilicity of primary imine calculated using the DFT's hybrid method mPWPW91 with toluene as the implicit solvent.

Entry	Substrate	Electrophilicity, ω (eV)
1		3.09
2		2.70
3		2.57
4		2.92
5		1.69
6		1.95
7		1.49
8		1.53
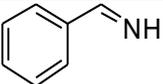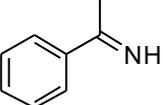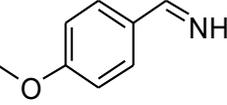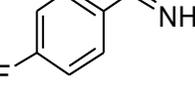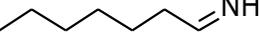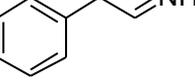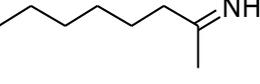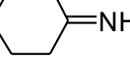
Table S-9. Characterization data of used 5% Pd-LDH (elemental composition, measured by ICP-AES).

Cycle (reaction)	Metal mol% (RSD)			
	Pd^{2+}	Mg^{2+}	Al^{3+}	M^{2+}/M^{3+}
Before use	4.53 (0.40)	70.5 (0.60)	24.8 (0.10)	2.98
Cycle 4 (coupling benzylamine)	4.13 (0.15)	70.7 (0.17)	25.2 (0.16)	2.8
Cycle 4 (dibenzylamine dehydrogenation)	3.83 (0.17)	70.6 (0.61)	25.6 (0.66)	2.8
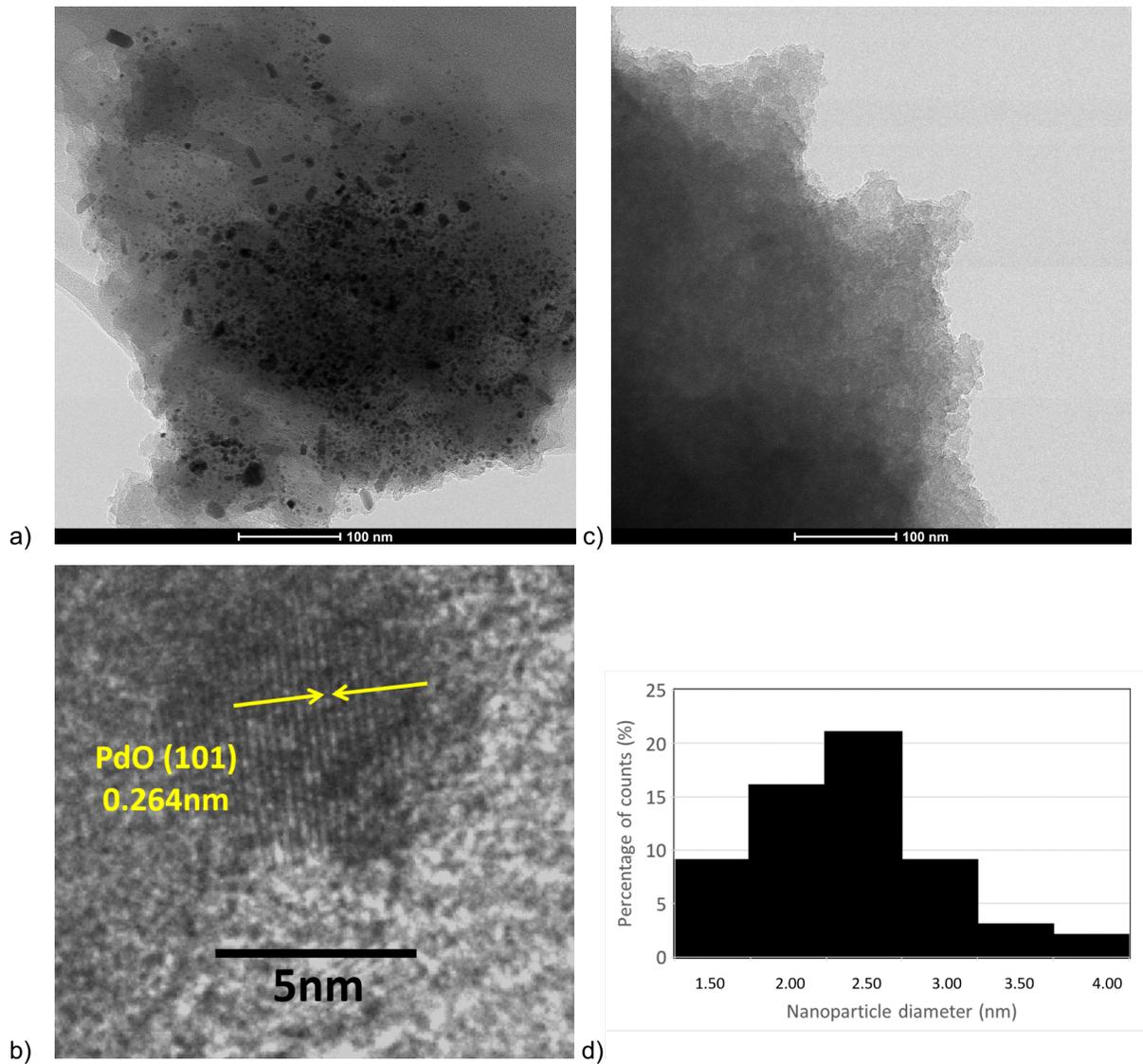
Figure S-9. (a & c) TEM image of used 5%Pd-LDH (**A**) (100 nm scale); (b**)** HRTEM and crystal lattice of used 5%Pd-LDH (**A**) showing a d-spacing of 0.234nm which indicates a higher Pd oxidation state. (d) Distribution of nanoparticle sizes of 3% Pd/C based on sampling of 500 particles.
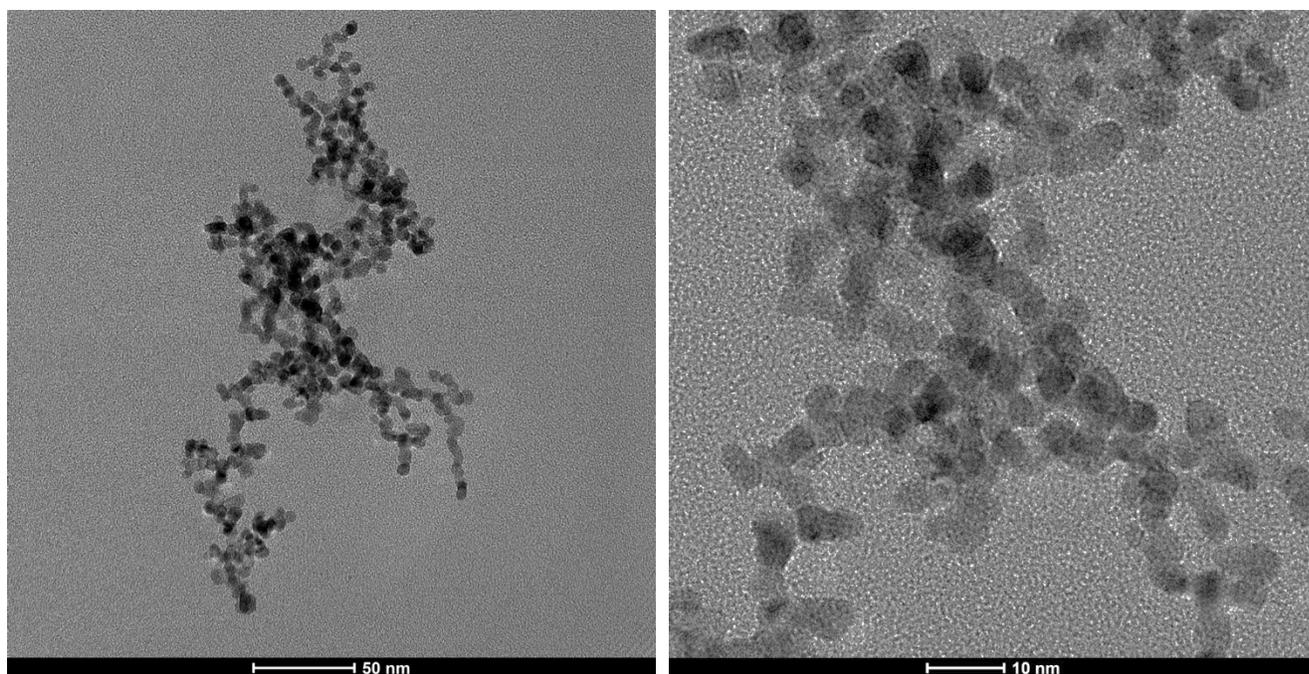
Figure S-10. TEM image of reaction mixture of Pd(OAc)$_2$ – Table 3, entry 7).

Table S-10. BET surface area, pore diameter and pore volume of 5% Pd-LDH (***A***) before and after use.

5% Pd-LDH (***A***)	BET Surface area, m^2/g	Pore diameter, Å	Pore volume, cm^3/g
Before use	52.8	66.1	0.132
After use	4.64	754.3	0.087

Experimental procedures for amine dehydrogenation reactions and reaction modeling:

1. Homocoupling of primary amines (Tables 2 and 3)

Microwave: in a typical procedure, a 10-mL microwave vial was charged with a stir bar, catalyst (mass calculated for 0.005 mmol Pd for Pd-LDH, and for Mg-Al LDH the mass was equal to that calculated for 0.5%Pd-LDH), amine (1 mmol) and 1 mL of toluene. The vial was sealed without exclusion of air, and the reaction was heated to 150 °C for the time indicated in a CEM Discover microwave reactor (maximum power = 300 W, stir rate: "high")". Yields determined by NMR and GC-FID using trimethoxybenzene as internal standard.

Conventional: a 20-mL reaction tube was charged with a stir bar, catalyst (mass calculated for 0.005 mmol Pd for Pd-LDH, and for Mg-Al LDH the mass was equal to that calculated for 0.5%Pd-LDH), amine (1 mmol) and 1 mL of xylenes. The mixture was heated to 140°C and allowed to run for up to 24 hours in a Heidolph Radleys Carousel 12 Plus Reaction Station. Yields determined by NMR and GC-FID using trimethoxybenzene as internal standard.

2. Dehydrogenation of secondary amines (Table 4)

Microwave: in a typical procedure, a 10-mL microwave vial was charged with a stir bar, 5%Pd-LDH (0.005 mmol, 10 mg), secondary amine (1 mmol) and 1 mL of toluene. The vial was sealed without exclusion of air, and the reaction was heated to 150 °C for 3 hours in a CEM Discover microwave reactor (maximum power = 300W, stir rate: "high"). Yields determined by NMR and GC-FID using trimethoxybenzene as internal standard.

Conventional: a 20-mL reaction tube was charged with a stir bar, 5%Pd-LDH (0.005 mmol Pd, 10mg), secondary amine (1 mmol) and 1 mL of xylenes. The mixture was heated to 140 °C and allowed to run for up to 24 hours in a Heidolph Radleys Carousel 12 Plus Reaction Station. Yields determined by NMR and GC-FID using trimethoxybenzene as internal standard.

3. Heterocoupling of primary amines

Microwave: in a typical procedure, a 10-mL microwave vial was charged with a stir bar, 5%Pd-LDH (0.005 mmol, 10 mg), benzylamine (1 mmol), amine 2 (2 mmol) and 1 mL of toluene. The vial was sealed without exclusion of air, and the reaction was heated to 150 °C for the time indicated in a CEM Discover microwave reactor (maximum power = 300W, stir rate: "high"). Yields determined by NMR and GC-FID using trimethoxybenzene as internal standard.

Conventional: a 20-mL reaction tube was charged with a stir bar, 5%Pd-LDH (0.005 mmol Pd, 10mg), benzylamine (1 mmol), amine 2 (2 mmol) and 1 mL of xylenes. The mixture was heated to 140 °C and allowed to run for up to 24 hours in a Heidolph Radleys Carousel 12 Plus Reaction Station. Yields determined by NMR and GC-FID using trimethoxybenzene as internal standard.

4. Catalyst recyclability

Conventional: following the reaction, the catalyst was centrifuged, and the supernatant was decanted off. The catalyst was washed with toluene, water, sodium bicarbonate (0.1M) and water. The catalyst was dried overnight at 110 °C. Elemental composition was determined using ICP-AES and the rest of the catalyst was used for another cycle of the same reaction.

5. Calculation of free energies of reaction (ΔG_{rxn})

All Calculations were performed using the Gaussian 16 program[4]. Geometries were minimized in toluene using the IEF-PCM implicit solvent model[5]; free energies were calculated at the B3LYP/6-31G* level of theory[6] at 423 K.

6. Calculation for electrophilicity

All Calculations were performed using the Gaussian 16 program[4]. The HOMO/LUMO energies were calculated using mPWPW91 hybrid method with the Gen basis set in toluene using the IEF-PCM implicit solvent model.[5]

NMR Characterization of products
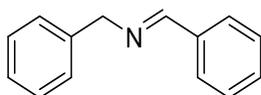
N-(phenylmethylene)benzenemethanamine: ^{1}H NMR (400 MHz, CDCl$_3$) δ = 4.80 (s, 2H), 7.19-7.32 (m, 1H), 7.32-7.33 (m, 4H), 7.37-7.41 (m, 3H), 7.76-7.78 (m, 2H), 8.36 (s, 1H).[7]
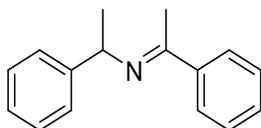
α-methyl-N-(1-phenylethylidene)benzenemethanamine: ^{1}H NMR (400 MHz, CDCl$_3$) δ = 1.44 – 1.32 (m, 3H), 2.61 (s, 3H), 4.16 (d, J = 6.6 Hz, 1H), 7.26 – 7.14 (m, 1H), 7.38 – 7.26 (m, 4H), 7.46 (ddd, J = 7.3, 4.0, 2.3Hz, 2H), 7.59 – 7.51 (m, 1H), 7.97 (d, J = 7.4 Hz, 2H).[8]
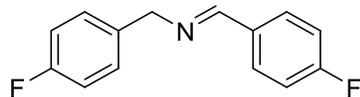
4-Fluoro-N-[(4-fluorophenyl)methylene] benzenemethanamine: ^{1}H NMR (400MHz, CDCl$_3$) δ = 4.75 (s, 2H), 6.99-7.04 (m, 2H), 7.06-7.10 (m, 2H), 7.26-7.30 (m, 2H), 7.74-7.77 (m, 2H), 8.32 (s, 1H).[9]
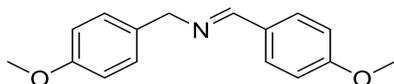
4-Methoxy-N-[(4-methoxyphenyl)methylene] benzenemethanamine: ^{1}H NMR (400MHz, CDCl$_3$) δ = 3.76 (s, 3H), 3.79 (s, 3H), 4.70 (s, 2H), 6.86 (d, J = 8.6 Hz, 2H), 6.90 (d, J = 8.7 Hz, 2H), 7.23 (d, J = 8.6 Hz, 2H), 7.70 (d, J = 8.7 Hz, 2H), 8.28 (s, 1H).[7]
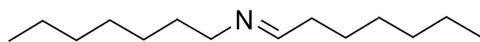
N-heptylideneheptanamine: ^{1}H NMR (400MHz, CDCl$_3$) δ = 0.85 (t, 6H), 1.25 – 1.65 (m, 16H), 2.37 (q, 2H), 3.84 (t, 2H), 7.40 (t, 1H).[10]
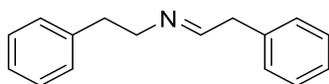
N-(2-phenylethylidene) benzeneethanamine: ^{1}H NMR (400 MHz, CDCl$_3$) δ = 1.73 (d, J=12.0, 2H), 2.87 – 2.73 (m, 2H), 3.01 – 2.88 (m, 2H), 7.34 – 6.97 (m, 10H), 7.51 (dd, J=13.6, 6.6, 1H).[11]
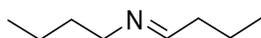
N-butylidenebutylamine: ^{1}H NMR (400 MHz, CDCl$_3$) δ = 0.7 – 1.1 (m, 6H), 1.2 – 1.9 (m, 6H), 2.0 – 2.5 (m, 2H), 3.25 (t, J = 6.5Hz, 2H), 7.78 (t, J = 4.8Hz, 1H).[12]
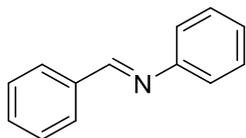
***N*-benzylideneaniline:** ^{1}H NMR (400 MHz, CDCl$_3$): δ = 8.52 (s, 1H, N=CH), 7.78-7.75 (m, 2H, H-arom), 7.31-6.98 (m, 8H, H-arom).[13]
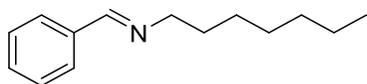
Benzylidene-heptyl-amine: ^{1}H NMR (400 MHz, CDCl$_3$): *δ* = 0.88 (t, *J* = 6.7 Hz, 2H), 1.28-1.35 (m, 8H), 1.66-1.73 (m, 2H), 3.59 (t, *J* = 7.0 Hz, 1H), 7.36-7.41 (m, 3H), 7.70-7.74 (m, 2H), 8.26 (s, 1H).[7]
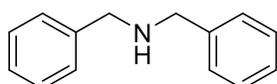
Dibenzylamine: ^{1}H NMR (400 MHz, CDCl$_3$): δ =3.68 (s, 4H), 7.21-7.24 (m, 2H), 7.30-7.36 (m, 8H).[14]
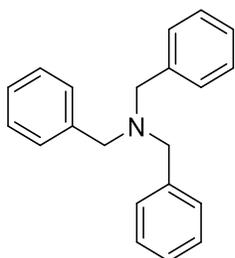
Tribenzylamine: ^{1}H NMR (400 MHz, CDCl$_3$): *δ* = 3.84 (s, 6H), 7.00-7.84 (m, 15H-Ar).[15]
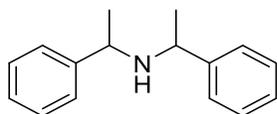
Bis(α-methylbenzyl)-amine: ^{1}H NMR (400 MHz, CDCl$_3$): δ = 1.27 (d, *J* = 6.7 Hz, 6H), 1.58 (br s, 1H), 3.49 (q, *J* = 6.7 Hz, 2H), 7.27–7.19 (m, 6H), 7.34–7.31 (m, 4H).[16]
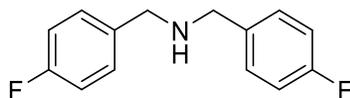
Bis(4-fluoro-benzyl)-amine: ^{1}H NMR (400 MHz, CDCl$_3$): δ = 1.58 (s, 1 H), 1.58 (s, 1 H), 3.75 (s, 4 H), 7.00 (t, *J* = 8.6 Hz, 4 H), 7.31-7.27 (m, 4 H).[17]
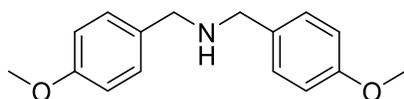
Dianisylamine: ^{1}H NMR (400 MHz, CDCl$_3$): δ = 3.68 (s, 4H), 3.75(s, 6H), 6.88-6.90 (d, 4H), 7.26-7.28 (d, 4H).[14]
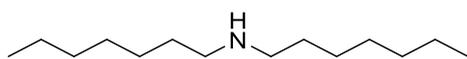
Diheptylamine: ^{1}H NMR (400 MHz, CDCl$_3$): δ = 0.90 (t, *J* = 7.0 Hz, 6H), 1.33 (m, 20H), 1.51 (m, 4H), 2.57 (t, *J* = 7.5 Hz, 4H).[18]
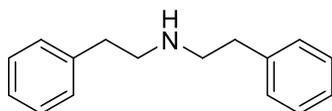
Diphenethylamine: ^{1}H NMR (400 MHz, CDCl$_3$): δ = 1.26 (s, 1 H), 2.78 (t, *J* = 7.2 Hz, 4 H), 2.89 (t, *J* = 7.1 Hz, 4 H), 7.21-7.15 (m, 6 H), 7.28-7.25 (m, 4 H).[17]
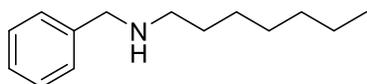
N-Benzyl-1-heptanamine: ^{1}H NMR (400 MHz, CDCl$_3$): δ = 0.81 (t, *J* = 7.0 Hz, 3 H), 1.22 (m, 8 H), 1.31 (m, 2 H), 1.52 (m, 2 H), 3.00 (t, *J* = 7.5 Hz, 2 H), 3.49 (s, br, 1 H), 6.51 (d, *J* = 7.5 Hz, 2 H), 6.60 (t, *J* = 7.5 Hz, 1 H), 7.09 (t, *J* = 7.5 Hz, 2 H).[18]

Pyridine: ^{1}H NMR (400 MHz, CDCl$_3$): δ = 6.91-6.96 (t, 2H), 7.30-7.35 (t, 1H), 8.29-8.33 (d, 2H).*
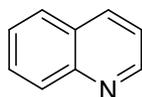
Quinoline: ^{1}H NMR (400 MHz, CDCl$_3$): δ = 7.38 (dd, *J* = 8.1, 4.2 Hz, 1H), 7.54 (t, *J* = 7.5 Hz, 1H), 7.71 (ddd, *J* = 8.4, 7.0, 1.4 Hz, 1H), 7.81 (d, *J* = 8.1 Hz, 1H), 8.13 (t, *J* = 9.3 Hz, 2H), 8.92 (dd, *J* = 4.2, 1.7 Hz, 1H).[19]
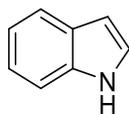
Indole: ^{1}H NMR (400 MHz, CDCl$_3$): δ = 6.58-6.54 (m, 1H), 7.15-7.09 (m, 1H), 7.23-7.17 (m, 2H), 7.23-7.17 (m, 2H), 7.40 (dd, J = 8.1, 0.8 Hz, 1H), 7.65 (dd, J = 7.9, 0.7 Hz, 1H), 8.1(brs, 1H).[19]

Key:
*Reference from NMR of pyridine of 99% purity from Acros.

References

1. R. Jenkins and R. L. Snyder, *Introduction to X-ray Powder Diffractometry*, John Wiley & Sons Inc., 1996.
2. J. F. Moulder, J. Chastain and R. C. King, *Handbook of x-ray photoelectron spectroscopy : a reference book of standard spectra for identification and interpretation of XPS data*, Physical Electronics, Eden Prairie, Minn., 1995.
3. K. S. Kim, A. F. Gossmann and N. Winograd, *Anal Chem*, 1974, **46**, 197-200.
4. M. J. Frisch, G. W. Trucks, H. B. Schlegel, G. E. Scuseria, M. A. Robb, J. R. Cheeseman, G. Scalmani, V. Barone, B. Mennucci, G. A. Petersson, H. Nakatsuji, M. Caricato, X. Li, H. P. Hratchian, A. F. Izmaylov, J. Bloino, G. Zheng, J. L. Sonnenberg, M. Hada, M. Ehara, K. Toyota, R. Fukuda, J. Hasegawa, M. Ishida, T. Nakajima, Y. Honda, O. Kitao, H. Nakai, T. Vreven, J. A. Montgomery, J. E. Peralta, F. Ogliaro, M. Bearpark, J. J. Heyd, E. Brothers, K. N. Kudin, V. N. Staroverov, R. Kobayashi, J. Normand, K. Raghavachari, A. Rendell, J. C. Burant, S. S. Iyengar, J. Tomasi, M. Cossi, N. Rega, J. M. Millam, M. Klene, J. E. Knox, J. B. Cross, V. Bakken, C. Adamo, J. Jaramillo, R. Gomperts, R. E. Stratmann, O. Yazyev, A. J. Austin, R. Cammi, C. Pomelli, J. W. Ochterski, R. L. Martin, K. Morokuma, V. G. Zakrzewski, G. A. Voth, P. Salvador, J. J. Dannenberg, S. Dapprich, A. D. Daniels, Farkas, J. B. Foresman, J. V. Ortiz, J. Cioslowski and D. J. Fox, *Journal*, 2009, DOI: citeulike-article-id:9096580.
5. J. Tomasi, B. Mennucci and E. Cances, *Theochem-J. Mol. Struct.*, 1999, **464**, 211-226.
6. W. J. Hehre, R. Ditchfield and J. A. Pople, *The Journal of Chemical Physics*, 1972, **56**, 2257-2261.
7. M. Lin, Z. Wang, H. Fang, L. Liu, H. Yin, C.-H. Yan and X. Fu, *RSC Adv.*, 2016, **6**, 10861-10864.
8. Y. Wang, F. Wang, C. Li and F. Jin, *International Journal of Hydrogen Energy*, 2016, **41**, 9128-9134.
9. G. F. P. de Souza, T. W. von Zuben and A. G. Salles, *ACS Sustainable Chemistry & Engineering*, 2017, **5**, 8439-8446.
10. H. A. Ho, K. Manna and A. D. Sadow, *Angew Chem Int Ed Engl*, 2012, **51**, 8607-8610.
11. J. Long, B. Yin, Y. Li and L. Zhang, *AIChE Journal*, 2014, **60**, 3565-3576.
12. R. Tanaka, M. Yamashita and K. Nozaki, *Journal of the American Chemical Society*, 2009, **131**, 14168-14169.
13. M. A. Esteruelas, V. Lezáun, A. Martínez, M. Oliván and E. Oñate, *Organometallics*, 2017, **36**, 2996-3004.
14. S. Lu, J. Wang, X. Cao, X. Li and H. Gu, *Chem Commun (Camb)*, 2014, **50**, 3512-3515.
15. M. Soleiman-Beigi and F. Mohammadi, *Monatshefte für Chemie - Chemical Monthly*, 2017, **148**, 2123-2128.
16. V. N. Wakchaure and B. List, *Angew Chem Int Ed Engl*, 2016, **55**, 15775-15778.
17. Z. Shao, S. Fu, M. Wei, S. Zhou and Q. Liu, *Angew Chem Int Ed Engl*, 2016, **55**, 14653-14657.
18. Z. Yin, H. Zeng, J. Wu, S. Zheng and G. Zhang, *ACS Catalysis*, 2016, **6**, 6546-6550.
19. J. Wu, D. Talwar, S. Johnston, M. Yan and J. Xiao, *Angew Chem Int Ed Engl*, 2013, **52**, 6983-6987.

ARTICLE

Acceptorless amine dehydrogenation and transamination using Pd-doped layered double hydroxides

An [a] Nan An,[a] Jinesh, C. Manayil,[b] Karen Wilson,[b] Adam F. Lee[b] and Adelina M. Voutchkova-Kostal*[a]

The synthesis, characterization, and activity of Pd-doped layered double hydroxides (Pd-LDHs) for for acceptorless amine dehydrogenation is reported. These multifunctional catalysts comprise Brønsted basic and Lewis acidic surface sites that stabilize Pd species in 0, 2+, and 4+ oxidation states. Pd speciation and corresponding cataytic performance is a strong function of metal loading. Excellent activity is observed for the oxidative transamination of primary amines and acceptorless dehydrogenation of secondary amines to secondary imines using a low Pd loading (0.5 mol%), without the need for oxidants. N-heterocycles, such as indoline, 1,2,3,4-tetrahydroquinoline, and piperidine, are dehydrogenated to the corresponding aromatics with high yields. The relative yields of secondary imines are proportional to the calculated free energy of reaction, while yields for oxidative amination correlate with the electrophilicity of primary imine intermediates. Reversible amine dehydrogenation and imine hydrogenation determine the relative imine:amine selectivity. Poisoning tests evidence that Pd-LDHs operate heterogeneously, with negligible metal leaching; catalysts can be regenerated by acid dissolution and re-precipitation.

Introduction

Acceptorless dehydrogenation (AD), the removal of molecular hydrogen from organic substrates without use of a sacrificial acceptor, is a highly desirable, atom-economical route to activating substrates and concomitant hydrogen production.[1] The development of efficient AD catalysts for various substrates would afford an alternative to synthetic methods that necessitate toxic reagents and produce stoichiometric waste. Furthermore, catalysts for AD may also facilitate hydrogen storage in organic molecules, as microscopic reversibility generally dictates that catalysts active for dehydrogenation also facilitate hydrogenation under a hydrogen pressure.

The development of catalysts for AD has received considerable attention for the production of alkenes from alkanes,[2] and carbonyls from alcohols.[3] Dehydrogenative coupling strategies have also been explored to afford long-chain alkanes, esters,[3c] amides, and secondary amines. However, in comparison to alcohols and alkanes, amines have been received less attention as substrates for AD, with the exception of N-heterocycles, which have been exploited for hydrogen storage.[4] Relative to the AD of cyclic compounds that can become aromatic upon dehydrogenation, AD of primary amines and acyclic secondary amines is thermodynamically more challenging. However, the dehydrogenation products of the latter, imines, are valuable intermediates that can be modified at the imine carbon, α-carbon, or nitrogen to form an array of amines and N-heterocycles.[5] Although aldimines can be prepared relatively easily via the condensation of aldehydes and primary amines, routes to ketimines require more arduous

conditions, such as the use of metal halides chlorides or other dehydrating agents to overcome the competing reverse reaction,[6] or use of Grignard reagents and nitriles.[7] Dehydrogenation of secondary amines could provide a valuable and atom-economical synthetic alternative to condensation routes. Existing methods for dehydrogenation of secondary amines include Swern oxidation, requiring strong oxidants,[8] or using catalytic pathways involving peroxides.[9] Dehydrogenative methods have also been developed using transfer hydrogenation of secondary amines with sacrificial hydrogen acceptors.[10] However, ultimately, methods that eliminate the need for oxidants or acceptors are highly desirable for mild synthetic conditions.

Primary amine dehydrogenation is also a synthetically useful route to secondary imines (Scheme 1b). This route has been referred to as oxidative transamination, and relative to the well-established alcohol-amine coupling route to imines (and amines), is nascent. Oxidative transamination of primary amines to form imines has been reported via photocatalytic routes[11] or in the presence of oxidants (e.g. H_2O_2,[12] AIBN,[13] t-butyl hydroperoxide,[14] TEMPO[15] or O_2[16]). Although it is highly desirable to eliminate the use of oxidants for this process, only two examples of homogeneous ruthenium catalysts have been reported that are active and selective for imine formation without oxidants, by Prades et al[17] and He et al.[18] However, due to the challenging nature of the reaction, catalysts reach only 90 turnovers in 20-48 h, and side products are often formed. Another Ru catalyst, reported by Blacquiere et al,[19] reached ~30 turnovers in 48 h, but with poor selectivity for imines over amines. On the heterogeneous front, Magyar et al reported that Cu(II) supported on molecular sieves facilitates the solventless selective coupling of imines,[20] and Torok et al reported that high loadings (1 g) of solid acidic K10 montmorillonite promoted

oxidative transamination under microwave conditions.[21] However, none of the preceding catalytically active sites are well-characterized, and none of the aforementioned systems facilitate dehydrogenation of acyclic and secondary amines.

Inspired by elegant examples of homogeneous catalysts that exploit ligand cooperativity, and several examples of supported Pd catalysts for dehydrogenation of N-heterocycles under mild conditions, we sought to develop heterogeneous catalysts active for the dehydrogenation of secondary amines and oxidative transamination of primary amines. Since ligand cooperativity has been recognized as a strategy for accessing lower energy pathways for homogeneous dehydrogenation systems,[22] we explored whether basic sites on a support surface may afford analogous cooperativity with catalytically active metal centres. Pd was selected in the latter regard, as supported Pd catalysts have shown promising recent activity in the dehydrogenation of N-heterocycles.[4] We postulated that dispersing Pd over a support that affords both high metal dispersion and allows tuning of acid/base sites proximal to Pd could enhance activity for dehydrogenation of heterocycles and even acyclic secondary amines. To this end, we targeted Pd-doped synthetic hydrotalcites (HTs).

HTs are layered double hydroxide (LDHs)[23] with a general formula of $[M^{2+}_{1-x}M^{3+}_x(OH)_2]_x+(A^{n-})_{x/n}.mH_2O$, where M^{2+} and M^{3+} are alkaline earth and transition metal cations, and A^{n-} represents interlayer anions. The surface acid/base,[24] redox,[25] and catalytic properties[26] of LDHs can be readily varied with composition, with minimal impact on morphology,[23] rendering them an intriguing choice of supports to optimize the activity and stability of dispersed phases. The LDH matrix can also support highly dispersed transition metal cations by incorporation in the cationic sheets or interlayers. We have recently developed a synthetic method that readily affords such dispersed species in LDHs using co-precipitation under continuous flow conditions. This immobilization strategy is distinct from that previously employed to support Rh,[27] Ru,[28] Ag,[29] Pd,[30] Au,[31] and Cu[32] by post-synthetic wet deposition on prepared HTs, which typically results only in nanoparticles. Pd incorporation into cationic LDH sheets has not previously been targeted to our knowledge.

Among the catalytic systems that consist of dispersed Pd on LDH or LDH-derived phases, Choudary et al reported that 4-6 nm Pd^0 nanoparticles (NPs) could be formed by reducing LDH impregnated with $PdCl_4^{2-}$ using hydrazine hydrate.[30a] Sivasanker et al reported that Pd immobilized on HT by post-synthetic wet deposition, but did show complete catalyst characterization.[33] There are also two examples of dispersed Pd phases on mixed metal oxide (MMO), derived by calcining LDHs, both synthesized by wet deposition. First, Chary et al[34] reported formation of PdO nanoparticles ~4 nm, which showed evidence of strong support interactions; and second, Tan et al demonstrated that Pd^0 nanoparticles on MMOs can be formed via a mild reduction method with alcohols.[30c]

Here we describe the synthesis and characterization of a class of Pd-LDH materials that exhibit distinct physicochemical properties from previously described examples due to the use of a new synthetic route. These materials show unique catalytic activity for acceptorless dehydrogenation of secondary amines (Scheme 1a) and oxidative transamination of primary amines via dehydrogenation (Scheme 1b).

Scheme 1
(a)
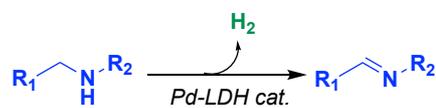
(b)
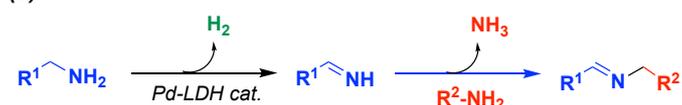
Results and discussion

Synthesis and characterization of Pd-LDHs

Pd-LDH catalysts with low and high Pd loadings (**A** and **B**) were synthesized using continuous flow precipitation (see ESI for details). Pd-free Mg-Al LDH (**C**) was also synthesized as a control via the same method.[35] Previously, our group had synthesized Pd-LDHs via two-step batch co-precipitation/wet deposition; however, the metal content of resulting materials was poorly reproducible, with standard deviations in the Pd, Mg, and Al molar ratios of up to 25 %. In contrast, the metal elemental composition of **A**, **B**, and **C** synthesized in flow are very reproducible, with standard deviations <5% of metal molar ratios (Table 1).

Powder XRD confirmed the presence of a single LDH phase, characterized by (003), (006), (009), (015), (018), (110) and (113) reflections (ESI Figure S-2a). The 2ϑ values of the (003), (006), and (009) reflections were used to estimate an average spacing between cation sheets (c), while the (110) and (113) reflections were used to estimate cation-cation distance within the cationic sheets (a) (ESI Table S2). The consistent a and c parameters in the three LDHs suggest that negligible differences in the layered structure arose due to Pd doping. No crystalline Pd phases were detected, even at the highest Pd loading (**A**), indicating that in all cases palladium was highly dispersed (either as low nuclearity species or <2 nm particles). Crystallite sizes, determined from line broadening using the Scherrer equation, were similar for the three materials (10.3-10.8 nm), suggesting agglomeration of nanocrystalline platelets.

FT-IR spectra of **A**–**C** show the expected characteristic bands for carbonate anions (1350-1370 cm^{-1}) and interlayer water (~1400 and 1700 cm^{-1}, ESI Figure S-2b), with no distinguishing characteristics for the Pd-doped LDHs.

Table 1 Average metal elemental composition of Pd-LDHs, as determined by ICP-AES.

Entry	Catalyst	Elemental comp. (metal mol%)[a] (σ)[b]		
		Pd	Mg	Al
1	5% Pd-LDH (**A**)	4.53 (0.17)	70.2 (1.0)	25.1 (0.50)
2	0.5% Pd-LDH (**B**)	0.53 (0.04)	73.1 (1.40)	25.6 (0.54)
3	Mg-Al LDH (**C**)	-	75.6 (1.52)	24.4 (0.45)

[a] Metal mol% is reported rather than mass% as the former is more appropriate for application to layered materials such as LDHs, for which interlayer anions and water exhibit dynamic behaviour; [b] σ is standard deviation from five batches.

Nitrogen porosimetry showed that **A**, **B**, and **C** possess Type IV isotherms, consistent with mesoporous solids.[36] **B** and **C** have type H3 hysteresis, which is associated with slit-like pores formed between aggregates of plates. TEM images confirm presence of microcrystalline plates in **A** and **B** (Figure 1). The hysteresis observed for **A** is type H2, which is associated with narrow-mouth, channel pores. TEM images of **A** show more aggregated particles, compared to the plates observed for **A** and **B** (Figure 1a). Furthermore, SEM images of a FIB-etched region of **A** show channel-like pores (ESI Figure S3).

The total BET surface areas of **A**, **B**, and **C** derived from nitrogen porosimetry data were 53, 155 and 144 m^2/g respectively. This trend was mirrored by the lower total pore volume for **A**, compared to **B** and **C** (ESI Table S-3). Thus, at low Pd loading the surface area and total pore volume of Pd-LDH (**B**) compares to that of the Pd-free LDH (**C**), but at the higher loading (**A,** 5% Pd) the pore volume and surface area significantly decreased. This decrease in surface area as a result of doping is significantly greater than that we have observed for doping with 15% of Cu, Ni, Co, Fe and Zn.

A pronounced difference was also observed between the pore size distributions **A** compared to **B** and **C**, calculated using the BJH method (Figure 2). While all three have mesopores in the range of 3 – 10 nm, A has significantly fewer pores in that range. Notably, all three have micropore volume that is negligible compared to the total BJH pore volume based on desorption data (ESI Table S-3).
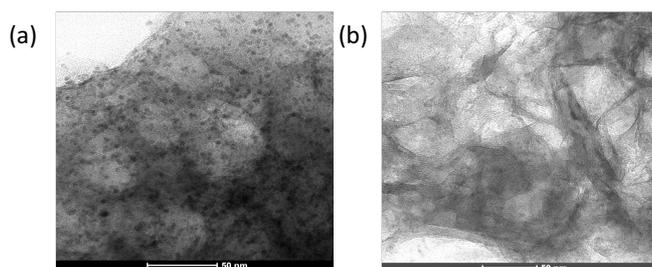
Figure 1 TEM images of (a) 5%Pd-LDH (**A**) and (b) 0.5%Pd-LDH (**B**). See ESI Figure S3 for more images and particle size distribution.
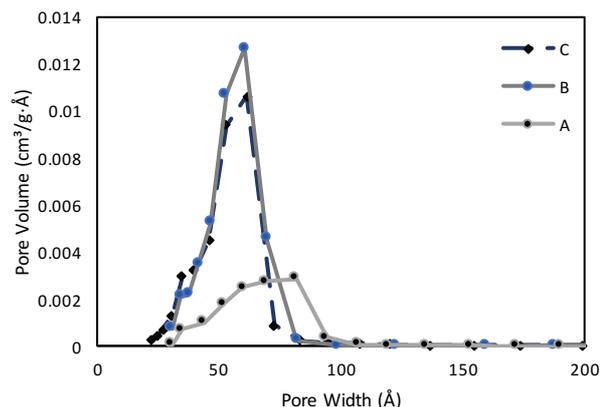
Figure 2 Pore size distributions for catalysts **A**, **B**, and **C**.

This, coupled with the fact that the interlayer spacing between hydrotalcite sheets (based on PXRD data) is ~ 2.3 nm (Table S-2), suggests that N_2 adsorption is measuring pores between clusters of particles. Since the crystallite sizes (based on PXRD data) are comparable for all three samples (10.3 – 10.8 nm), we attribute the presence of fewer and more widely distributed pores in **A** to faster rate of the agglomerated particle growth compared to **B** and **C**. This is consistent with our observation of faster precipitation during ageing in the case of **A**.

All three LDHs exhibit characteristic thermal decomposition profiles of this class of materials, with three endothermic transitions: at T <100 °C (I), representing the loss of physisorbed water, at T ~ 150 °C (II), corresponding to the loss of interlayer water, and at T ~ 350-450 °C, corresponding to dehydroxylation and decarbonation processes (III).[23] The temperatures of these transitions vary significantly with LDH composition, and signify changes in thermal stability of the LDH. The order of stability of LDH samples is **C** > **B** > **A** (Figure 3), thus decreasing with increasing Pd content. This trend is consistent with the expectation that LDH without dopants (**C**, hydrotalcite) is the most stable, and cation substitution creates disorder and structural changes. The thermal stability of the LDH also depends on the stability of the incorporated cation in a particular oxidation state.[37]

Temperature programmed desorption (TPD) was used to determine the temperature associated with carbonate loss as CO_2. Although the differences in the temperatures associated with loss of CO_2 for the three materials are not large (451 °C for **A**, 462 °C for **B** and 458 °C for **C**, ESI Figure S4), we found a direct correlation between these and the total BET surface area ($R^2 = 0.93$) and the pore volume calculated from N_2 desorption ($R^2 = 0.99$, ESI Figure S5). This relationship suggests could arise through the effect of thermodynamic stability on rate of agglomeration of platelets, namely, that lower stability of the LDH results in slower aggregation, better stacking and thus formation of fewer mesopores.

Given that LDHs are known to have strong Lewis and Bronsted base sites, in addition to weak Lewis acidic sites, we examined potential differences between the acid-base

properties of *A, B* and *C.* The base site density was determined by CO_2 pulse titration. The total molar quantity of CO_2 adsorbed per gram of LDH showed an inverse relationship with the Pd doping (Figure 4) – dropping almost 4-fold with 5% Pd doping relative to the Pd-free LDH. Given that the LDHs contain interlayer carbonates, which are released upon heating as CO_2, TPD data with CO_2 as probe does not directly reflect the distribution of strength of acidic sites.

To probe the acidic sites, temperature programmed desorption (TPD) was carried out on the three materials using a reactive probe - isopropylamine, to investigate distribution of acidic sites. Isopropylamine undergoes Hoffman elimination over accessible acidic sites to form propylene. As such, it is a more discriminate probe for acidic sites relative to ammonia, whose strong basicity and small size often result in overestimates of the density of acidic sites. TPD using isopropylamine, a relatively new technique, has not to the best of our knowledge been previously applied to the study of LDHs.
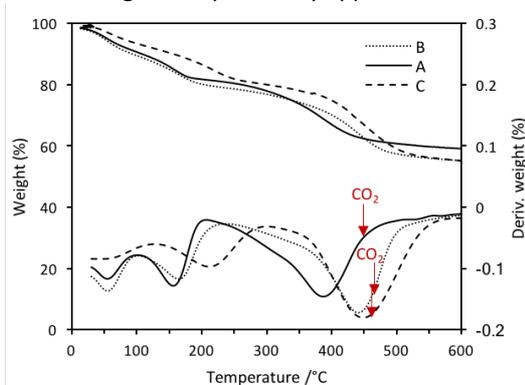

Figure 3.TGA-DTG curves for the Pd-LDHs A and B and LDH C. Red arrows show temperature at which TPD indicates loss of carbonate as CO_2.
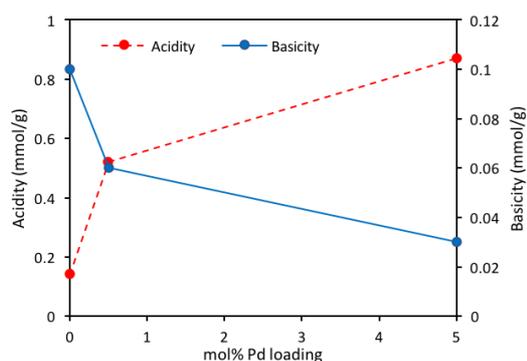
Figure 4 Total acidity and basicity vs Pd loading for catalysts *A*, *B* and *C*.
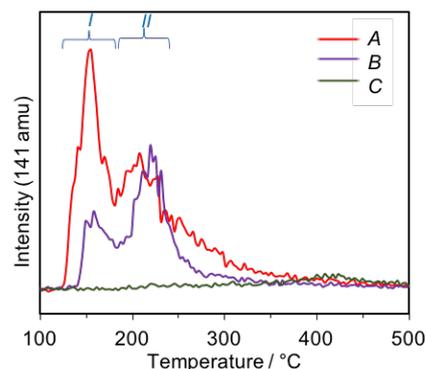
Figure 5 Temperature programmed desorption of *A*, *B* and *C* using isopropylamine, which form propylene (amu 141) over accessible acidic sites.

TPD profiles of propylene (formed via elimination of iso-propylamine) showed no transformation over Pd-free LDH, *C* (Figure 5). In contrast, Pd-LDHs (*A* and *B*) show release of propylene at 120 – 180 °C (range *1* in Figure 5), 180 – 240 °C (range *2*) and temperatures > 250 °C. The quantity of propylene released by *A* in range 1 exceeds significantly that by *B*, suggesting that the number of active sites for this process are proportional to quantity of Pd. However, quantity of propylene released in range 2 is comparable for *A* and *B,* suggesting the active sites associated are independent of Pd content. The latter may be the case if the sites occur at the juncture between Pd and Mg or Al. The total acid site density, estimated by integrating the total desorption peak area, varies substantially with Pd doping, ranging from 0.14 mmol/g for *C*, to 0.87 mmol/g for *A*, and is related to the Pd content (Figure 4).

X-ray photoelectron spectroscopy (XPS) showed different Pd speciation for the two Pd-LDHs (Figure 6, and see ESI Table S-4 for tabulated data). *A* and *B* contain two common Pd chemical environments: one with a $3d_{5/2}$ binding energy of 336.3 eV, and the second with a $3d_{5/2}$ binding energy of BE of 338.2 eV. The former is characteristic of Pd^{2+},[38] and latter of Pd^{4+}.[27] A third chemical environment indicative of Pd^0 with a $3d_{5/2}$ binding energy of 335.3 eV was also observed for *A* (5%Pd-LDH). The speciation of these states for *A* was Pd^{4+}(17): Pd^{2+}(58): Pd^0(25), while that in *B* was the relative abundance of Pd^{4+}(34): Pd^{2+}(66) (Figure 6). LDHs thus offer multiple coordinating environments for Pd, two for *B* and three for *A*. These observations contrast with reports of post-synthetic immobilization of Pd on LDHs and mixed metal oxides, wherein a single Pd species was observed.[30a, 34] The high concentration of Pd^{4+} species in *B* suggests strong support interactions, consistent with the lower Pd loading and hence higher metal dispersion anticipated.
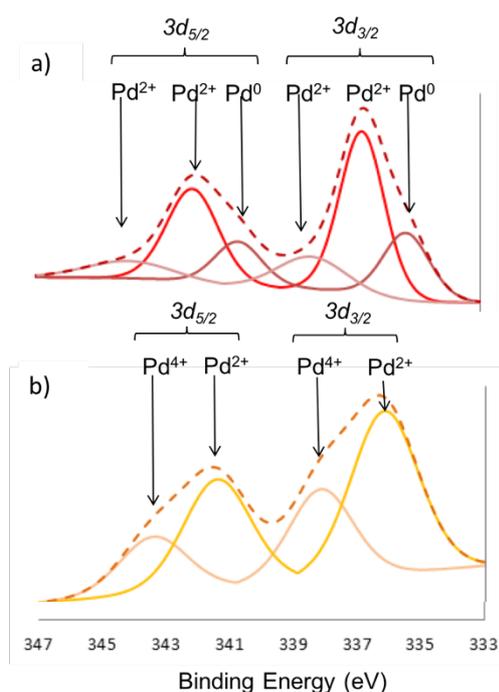
Figure 6 X-ray photoelectron spectra of (a) *A* (5%mol Pd-LDH) and (b) *B* (0.5%mol Pd-LDH).

only resulted in a small increase in the Pd^0 population with Pd^{4+}(28): Pd^{2+}(50): Pd^0(22) observed. The present stabilisation of high oxidation state palladium in Pd-LDHs materials synthesized in flow distinguishes them from literature examples of palladium supported over LDHs or mixed metal oxides.

Secondary amine dehydrogenation

The activity of *A*, *B* and *C* for acceptorless dehydrogenation (AD) of a model secondary amine, dibenzylamine, was explored under reflux in *p*-xylene for 24 h using 0.5 mol% Pd relative to the amine. Under these conditions, *A* afforded 93 % imine, compared to 41 % for *B*, and only a negligible yield for the bare support *C*. The superior activity of *A* suggests that Pd^0 may be the most active Pd phase for dehydrogenation. The same results were obtained under an inert atmosphere, confirming that residual oxygen played no role. *A* outperformed soluble $Pd(OAc)_2$, which only afforded 72 % imine (Table 2, entry 7). The latter reaction mixture was examined on TEM post-reaction, and Pd nanoparticles of size 4-8 nm were observed (ESI Figure S9). Meanwhile, commercial Pd/C, which was found by TEM to comprise of 5-30 nm Pd^0 NPs, afforded marginally lower yields and showed significant variability depending on the batch and manufacturer.

TEM images of *A* and *B* were consistent with XRD and XPS, with no nanoparticles observed for *B*, and only 1-2.5 nm Pd NPs observed for *A* (Figure 2 and ESI Figure S3). HRTEM images identified two types of NPs in *A*, those with lattice fringes of 0.227 nm corresponding to *fcc* Pd(111) facets, and those with lattice fringes of 0.215 nm corresponding to PdO(110) facets (ESI Figure S-4).
.
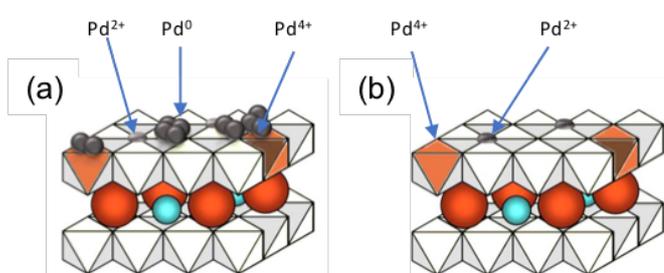
Figure 7. Schematic of Pd species in (a) *A* and, (b) *B* Pd-LDHs.

Based on XPS, TEM, and the ionic radii data of Pd in different oxidation states, we propose that the low loading Pd-LDH, *B*, consists of Pd^{4+} species either incorporated into the LDH matrix and surface bound Pd^{2+} low nuclearity species (Figure 7). Pd-LDH *A* also consists if these two species, in addition to highly dispersed metallic Pd nanoparticles, which likely nucleate when the palladium loading reaches a critical threshold and Pd-Pd interactions become significant. We hypothesized that the highly dispersed oxidized Pd species, being stabilised by a strong metal support interaction, would be resistant to reduction to Pd^0. Indeed, attempts to reduce Pd^{2+} and Pd^{4+} in *A* using $NaBH_4$

Table 2 Yields of *(E)-N*-benzylidene-1-phenylmethanamine from dehydrogenation of dibenzylamine using Pd catalysts.
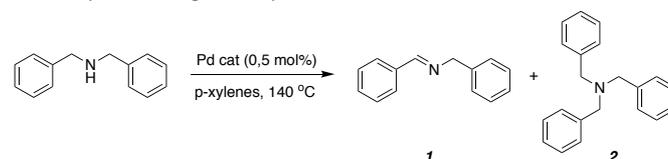
Entry	Catalyst	Yield %		Conv. %
		Imine (**1**)	3° amine (**2**)	
1	5% Pd-LDH (**A**)	95 (±4)	0	>98
2	0.5% Pd-LDH (**B**)	41 (±7)	0	58
3	Mg-Al LDH (**C**)	0	0	0
4	Calcined **A**	80 (±5)	17	>98
5	Calcined **B**	48 (±7)	20	70
6	5% Pd/C	83 (±10)	9	>98
7	Pd(OAc)₂	72 (±4)	2	75

Conditions: 1 mmol of benzylamine, 0.5 mol% Pd loading, 1 mL p-xylene, 4 h at 140 °C; yields determined using an internal standard by NMR and GC-FID.

The applicability of *A* was subsequently explored for other secondary amines under the same conditions (Table 3). Excellent yields were obtained with secondary benzylamines (80-93 %, entries 1-2) and an aliphatic amine (dibutylamine, 72%, entry 5).

Table 3 Acceptorless dehydrogenation of secondary amines using 0.5 mol% catalyst **A**.

Entry	substrate	product	Yield %	TON
1			93	186
2			80	160
3[a]			83	83
4[a]			72	144
5			72	144
6[a]			45	135
7			27	54
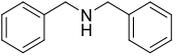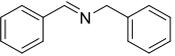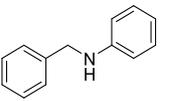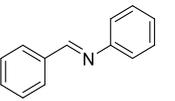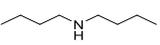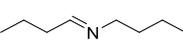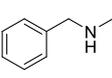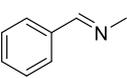
Conditions: Substrate (1 mmol), 10.0 mg catalyst **A** (0.0.5 mol% Pd), *p*-xylenes (1 mL), 140 °C under 24 h reflux; yields determined using an internal standard by NMR and GC-FID. [a] 1 mol% Pd loading.

AD was also performed on *N*-heterocycles (Table 3, entries 3, 4, and 6). Indoline and 1,2,3,4-tetrahydroquinoline were dehydrogenated with excellent yields (83 % and 72 % respectively) to the corresponding aromatic compounds indole and quinolone. For 1,2,3,4-tetrahydroquinoline this requires removal of two H_2 equivalents, equating to 144 turnovers. Piperidine afforded a 45 % yield of pyridine in 24 h (135 turnovers for the three dehydrogenative steps per molecule), which is highly competitive with existing homogeneous catalysts.[39] Relative yields of the three heterocycles are consistent with computed free energies of their reactions (ΔG_{rxn}, B3LYP/6-31G(d) of -11.29, -6.79 and 0.50 kcal/mol) respectively for indoline, tetrahydroquinoline and piperidine respectively (see ESI for computational details and ESI Table S5, entries 6-8).

Oxidative Transamination

Reactions with primary amines afford the selective formation of secondary imines. This reaction proceeds via dehydrogenation of the primary amine to form a reactive aldimine, which undergoes nucleophilic attack by another amine to form the secondary imine and concomitant elimination of NH_3 (Scheme 1b). Gases liberated during the reaction were identified as H_2 and NH_3 by splint test and GC-MS respectively.

Using the same reaction conditions as above (0.5 mol% Pd, 140 °C), catalyst **A** afforded >90 % yield of the secondary imine in 4 h, with <5 % secondary amine (Table 4, entry 1). This is a

significant improvement over homogeneous systems under comparable conditions.[17-19] No nitrile formation was observed, suggesting that a second dehydrogenation of the aldimine[40] is slower than transamination. The secondary amine starts to form immediately, implying facile hydrogenation of the secondary imine. After 2 h reaction, the secondary amine concentration decreases, indicating that it undergoes a slow subsequent dehydrogenation (Figure 4a). Catalyst **B** yielded 56 % imine in 5 h, with complete conversion. The mass imbalance implies that some substrate or product is retained on the LDH (Figure 4c), and may reflect the larger mass of catalyst **B** required to achieve the same 0.5 mol% Pd:substrate loading to mirror that employed for **A**. In comparison, under the same conditions Pd/C afforded 75 % imine and 25 % tertiary amine, and only 50 % imine with $Pd(OAc)_2$ in 4 h (entries 4-5). The Pd-free LDH support **C** formed no products (entry 3), confirming that the acid-base sites alone on the support do not effectively catalyse the reactions.

Table 4 Yields of *(E)-N*-benzylidene-1-phenylmethanamine (*1*) and dibenzylamine (*2*) from dehydrogenative coupling of benzylamine (below).
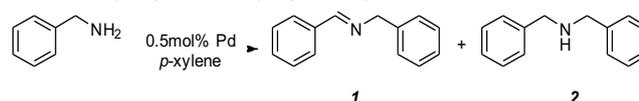
Entry	Catalyst	Yields		Conversion
		Imine (*1*)	Amine (*2*)	
1	5% Pd-LDH (**A**)	93	<5	>98
2	0.5% Pd-LDH (**B**)	56	<5	>98
3	Mg-Al LDH (**C**)	<5	0	8
4	5% Pd/C	75[a]	0	<98
5	$Pd(OAc)_2$	50	17	70

[a]25% yield of tertiary amine (yield calc based on theoretical yield of tertiary amine). Conditions: 1 mmol of benzylamine, 0.5 mol% Pd loading of catalyst, 1 mL p-xylene, 24 hrs at 140 °C; yields determined using an internal standard by NMR and GC-FID.

Reactions performed under microwave conditions at 150 °C in a closed vial resulted in almost identical yields to those in Table 3. However, small amounts of secondary amine (from hydrogenation of the secondary imine) were observed, which slightly lowered imine selectivity (Figure 8b and d). This likely reflects the release of reactively-formed hydrogen possible under reflux conditions, which minimizes imine hydrogenation.

Self-coupling of amines under these conditions was also explored for a series of primary amines. Overall, conventional heating resulted in higher selectivity than microwave heating (Table 4). All benzylamines tested (entries 1-4) afforded high conversion and high selectivity, yielding 72-97 % imine, consistent with formation of a primary imine that is stabilized by conjugation with the benzene ring. Electron-withdrawing and donating substituents did not significantly affect yields, which was surprising given that homogeneous Ru catalysts exhibit lower activity with substituted benzylamines.[17-18] Alkyl amines afforded lower yields of secondary imine than benzylamines with lower imine:amine selectivity (~2:1, entry 5). The lower imine selectivity may result from faster secondary

imine hydrogenation relative to other substrates. The two substrates with substitution at the α-position, which form

(a)

(b)

(c)

(d)
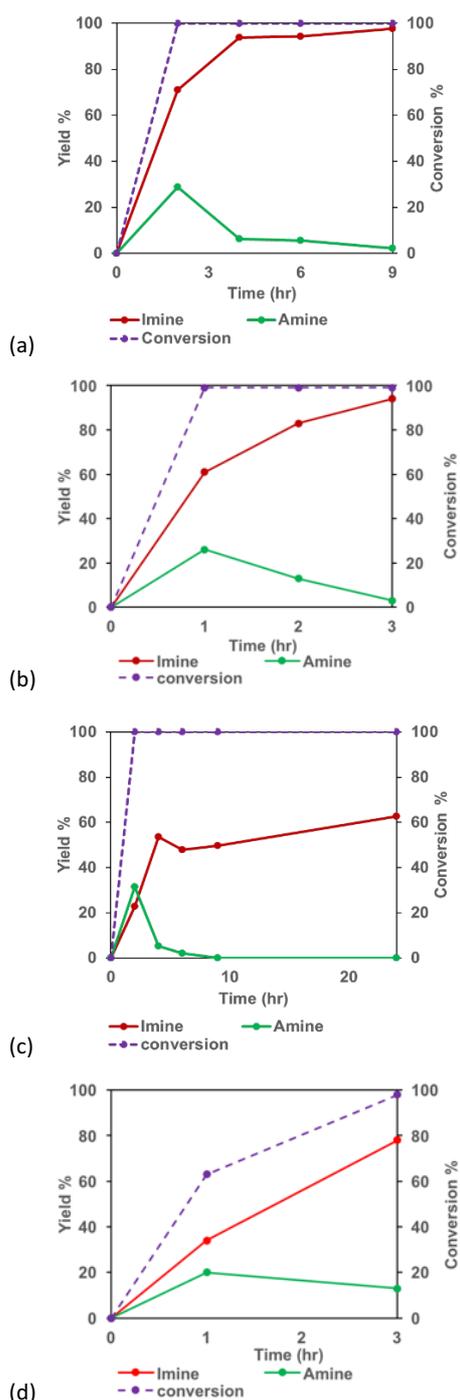
Figure 8 Reaction profiles for dehydrogenative coupling of benzylamine to form imine (**1**) and amine (**2**) using 0.5 mol% loading of **A** in (a) conventional heating; (b) microwave heating; and using 0.5 mol% loading of **B** in (c) conventional heating and (d) microwave heating.

ketimines when dehydrogenated, had lower yields compared to those that form aldimines (entries 2 and 7).

Table 4 Substrate scope for oxidative transamination of amines using catalyst **A**. For yields using microwave heating see ESI Table S-6.
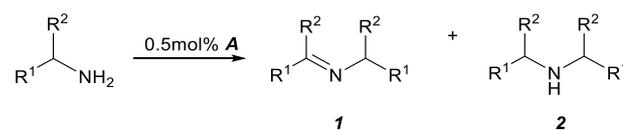
| Entry | R^1 | R^2 | Yield % | | Dehydrog. |
			1	**2**	TON[a]
1	Ph	H	97	0	209
2	Ph	Me	72	0	144
3	Ph(p-OMe)	H	91	0	182
4	Ph(p-F)	H	95	0	190
5	hexyl	H	57	28	95
6	Ph(CH$_2$)	H	33	19	66
7	hexyl	Me	5	0	10
8	cyclohexyl	H	5	0	10

Conditions: substrate (1 mmol), catalyst **A** (0.005 mol Pd), p-xylenes (1 mL), conventional heating with p-xylenes as the solvent for 24 hr at 140 ^{o}C. Yields determined using an internal standard by NMR and GC-FID. [a]Average TON for primary amine dehydrogenation estimated from catalyst mass, assuming all Pd species were active.

The relationship between relative yields for the substrates in Table 4, and computed electronic parameters and free energy of reaction, calculated using the DFT hybrid method mPWPW91, (see ESI for details) was also investigated. Electrophilicity of the primary imine intermediate (ω, see ESI Table S-8) correlates strongly to the turnover numbers (TONs) and yields of imine obtained (Figure 9, $R^2 = 0.90$). Although this trend does not imply causality or identifies the rate-determining process in the 2-step reaction (Scheme 1b), it does offer a facile means to estimate the relative reactivity of new substrates.
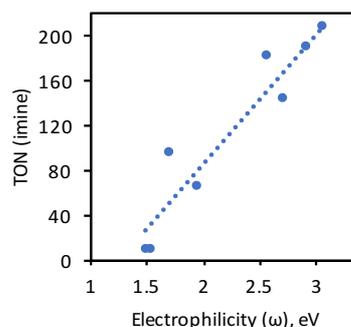
Figure 9 TON (based on imine formation using catalyst A) and computed electrophilicity index (ω) of the respective primary imine intermediates. Coefficient of determination (R2) = 0.90.

Heterocoupling of amines was also explored using the above protocol. In the coupling of heptylamine with benzylamine (Scheme 2), reaction proceeded to full conversion of benzylamine and exclusively afforded the heterocoupled product. As anticipated from prior results, the imine selectivity obtained under conventional reflux, wherein liberated H$_2$ can escape, is higher than that obtained with microwave heating in a closed vial (imine:amine = 63:37 vs 54:44 for conventional vs

microwave heating respectively). Under conventional heating, full conversion of benzylamine is reached in only 1 h, with longer reactions favoring dehydrogenation of the secondary amine to imine (Figure 10). A further increase in reaction time would therefore be anticipated to increase selectivity to the imine.

Scheme 2

toluene, mw, 150 °C, 3h: 54%   44%
xylenes, conv, 140 °C, 24h: 63%   37%
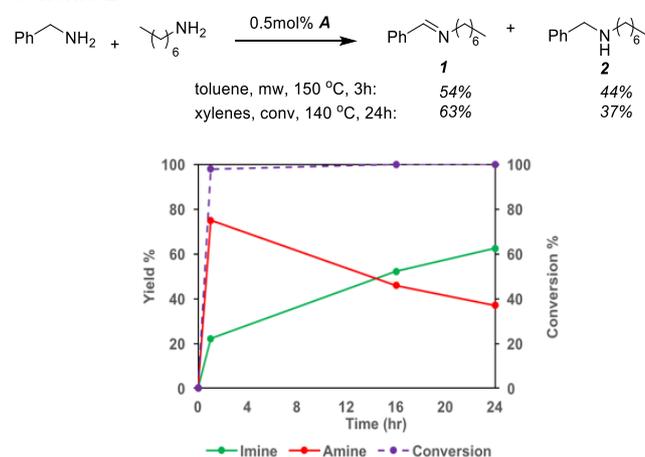
Figure 10 Reaction time course for dehydrogenative coupling of benzylamine and heptylamine using 5%Pd-LDH (**A**).

Heterogeneity tests

To investigate whether catalysts **A**-**C** are operationally heterogeneous, we applied a combination of hot filtration, selective poisoning, and mercury poisoning tests. A three-phase test was also attempted, but could not yield definitive results in our hands due to decomposition of the amines upon hydrolysis from the silica support used to immobilize the substrate.

Hot filtration was performed by sampling a portion of the reaction mixture containing benzylamine and catalyst **A** after 30 min reaction and passing this through a hot frit. After 5 h further reaction, product concentrations in the filtrate and control (catalyst containing) reactions were compared. While the control showed near quantitative conversion to the imine, the imine and amine concentrations in the filtrate did not change; catalytically active species are absent from the filtrate. However, this test is not definitive, since rapid re-deposition of catalytically active species ("catch and release") can occur upon even partial cooling of the reaction during filtration.[41] We therefore also examined the effect of a known scavenger for soluble palladium species, Quadrapure-TU,[42] (a polystyrene resin with thiourea functionality) on the benzylamine oxidative amination with **A**. We note that some of the co-authors have previously shown that Quadrapure-TU not only scavenges soluble Pd complexes, but also soluble Pd nanoparticles.[43] The progress of reaction in the presence of excess Quadrapure-TU was identical to a conventional reaction with no significant differences in 24 h imine yields (93 % vs 97 % for reactions with and without Quadrapure-TU respectively). This result is consistent with the hot filtration test, suggesting that the reaction is likely not catalysed by soluble Pd species. However,

it is not possible to rule out that Quadrapure-TU may not be effective at scavenging soluble Pd species ligated with amines, and there is also evidence that porous silicas, whether thiolated or unfunctionalised, do not select for soluble palladium but also trap nanoparticles.[43]

Since mercury is expected to amalgamate supported palladium species, thus eliminating their activity,[43] we also performed a mercury poisoning experiment. In the presence of mercury only 6 % yield of secondary imine was obtained, suggesting that the catalytically active species was effectively poisoned. The results of the three tests are consistent with operationally heterogeneous catalysts. However, given that we were unable to obtain definitive results from the three-phase test, future operando spectroscopic studies will be performed to further interrogate the nature of the catalytic species.

Recyclability

Catalyst recycling was undertaken by post-reaction centrifugation and sequential washing of the recovered solid with toluene, aqueous sodium bicarbonate, and then water, prior to drying overnight. TONs for four consecutive cycles were compared for both reaction classes (Figure 11).
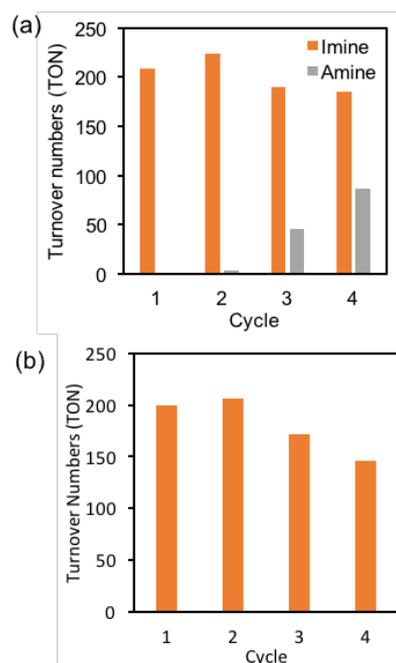
Figure 11 Recyclability of catalyst **A** in (a) the dehydrogenative coupling of benzylamine and (b) the dehydrogenation of dibenzylamine.

Catalyst **A** retained ~90 % of its activity over four cycles of benzylamine oxidative transamination (Figure 7a). However, a decrease in selectivity for imine was observed in cycles 3 and 4, suggesting that activity for secondary amine dehydrogenation was suppressed. This was corroborated by data comparing the activity of **A** for the dehydrogenation of dibenzylamine for which activity decreased by 5 % and 25 % in cycles 3 and 4 respectively (Figure 7b).

To test whether this activity loss was associated with Pd leaching, the elemental composition of **A** before and after multiple cycles was determined. After four cycles of benzylamine coupling, the change in Pd, Mg, and Al mol% and molar ratios were within the standard error (ESI Table S-9). PXRD also showed no change in catalyst morphology post-reaction. Since Pd leaching is unlikely to be the major cause of the observed selectivity change, we subsequently examined Pd speciation before and after reaction. TEM images of the catalyst after four cycles evidenced PdO formation (ESI Figure S-5), indicating that some of the initial Pd0 species underwent oxidation，thereby reducing the catalyst dehydrogenative activity. Further detailed studies are needed to elucidate the nature of the catalytically active species and oxidation kinetics.

However, given that significant metal leaching does not occur, we can regenerate the catalyst by dissolving in nitric acid and re-precipitating the Pd-LDH using sodium carbonate and hydroxide. This is an advantageous feature of LDHs, which differentiates them from most other supported Pd catalysts.

Conclusions

Acceptorless amine dehydrogenation is a promising atom-economical route to functionalized amines and imines, but with few catalytic examples. Here we report the development of a new class of supported Pd doped layered double hydroxide (Pd-LDHs), which are active for acceptorless amine dehydrogenation, and hold promise as tunable heterogeneous Pd catalysts. 5 mol % Pd-LDH (**A**) exhibits excellent activity for secondary amine dehydrogenation and oxidative transamination of primary amines at low catalyst loadings (0.5 mol% relative to substrate), and affords excellent yields with secondary benzyl and alkylamines. *N*-heterocycles (indoline, 1,2,3,4-tetrahydroquinoline and piperidine) were also dehydrogenated to the corresponding aromatic compounds with high yields. Catalyst **A** is also active for oxidative amination of primary amines to imines. Benzylamines afforded high yields and high selectivity for the secondary imine, while alkyl amines afforded lower yields due to lower imine:amine selectivity. The relative activity directly correlates with the calculated electrophilicity of the primary imine intermediates. Heterocoupling of aliphatic and benzylic amines is also demonstrated.

Strong evidence is presented that catalysis is entirely heterogeneous, however a catch-and-release mechanism cannot be entirely excluded at present. Catalyst A retained ~90 % activity over four cycles of oxidative amination, accompanied by a small decrease in selectivity for imine reflecting a decline in secondary amine dehydrogenation due to partial oxidation of metallic Pd to PdO. However, catalytic performance could be regenerated by acid dissolution and re-precipitation.

Conflicts of interest

There are no conflicts to declare.

Notes and references

1. (a) Gunanathan, C.; Milstein, D., *Science* **2013,** *341* (6143), 249-+; (b) Dobereiner, G. E.; Crabtree, R. H., *Chem Rev* **2010,** *110* (2), 681-703.
2. (a) Kumar, A.; Bhatti, T. M.; Goldman, A. S., *Chemical Reviews* **2017,** *117* (19), 12357-12384; (b) Goldman, A. S.; Krogh-Jespersen, K.; Brookhart, M., *Abstr Pap Am Chem S* **2011,** *242*; (c) Crabtree, R. H.; Mihelcic, J. M.; Quirk, J. M., *Journal of the American Chemical Society* **1979,** *101* (26), 7738-7740.
3. (a) Zhang, J.; Balaraman, E.; Leitus, G.; Milstein, D., *Organometallics* **2011,** *30* (21), 5716-5724; (b) Fujita, K.; Tamura, R.; Tanaka, Y.; Yoshida, M.; Onoda, M.; Yamaguchi, R., *Acs Catalysis* **2017,** *7* (10), 7226-7230; (c) Nielsen, M.; Junge, H.; Kammer, A.; Beller, M., *Angew Chem Int Edit* **2012,** *51* (23), 5711-5713; (d) Musa, S.; Shaposhnikov, I.; Cohen, S.; Gelman, D., *Angew Chem Int Edit* **2011,** *50* (15), 3533-3537.
4. (a) Moores, A.; Poyatos, M.; Luo, Y.; Crabtree, R. H., *New J Chem* **2006,** *30* (11), 1675-1678; (b) Crabtree, R. H., *Energy & Environmental Science* **2008,** *1* (1), 134-138; (c) Cui, Y.; Kwok, S.; Bucholtz, A.; Davis, B.; Whitney, R. A.; Jessop, P. G., *New J Chem* **2008,** *32* (6), 1027-1037.
5. Lawrence, S. A., *Amines : synthesis, properties, and applications*. Cambridge University Press: New York, 2004; p x, 371 p.
6. Billman, J. H.; Tai, K. M., *J. Org. Chem.* **1958,** *23* (535-537).
7. Weiberth, F. J.; Hall, S. S., *J Org Chem* **1987,** *52* (17), 3901-3904.
8. Keirs, D.; Overton, K., *J. Chem. Soc. Chem. Commun.* **1987,** *18* (1660-1661).
9. (a) Mare, H. E. D. L., *The Journal of Organic Chemistry* **1960,** *25* (12), 2114-2126; (b) Murahashi, S.-I.; Naota, T.; Taki, H., *Journal of the Chemical Society, Chemical Communications* **1985,** (9), 613-614.
10. Gu, X. Q.; Chen, W.; Morales-Morales, D.; Jensen, C. M., *J Mol Catal a-Chem* **2002,** *189* (1), 119-124.
11. (a) Zhai, Z. Y.; Guo, X. N.; Jin, G. Q.; Guo, X. Y., *Catal Sci Technol* **2015,** *5* (8), 4202-4207; (b) Lang, X. J.; Ji, H. W.; Chen, C. C.; Ma, W. H.; Zhao, J. C., *Angew Chem Int Edit* **2011,** *50* (17), 3934-3937.
12. Chu, G.; Li, C., *Organic & Biomolecular Chemistry* **2010,** *8* (20), 4716-4719.
13. Liu, L. H.; Wang, Z. K.; Fu, X. F.; Yan, C. H., *Organic Letters* **2012,** *14* (22), 5692-5695.
14. Zhang, Z.; Wang, F.; Wang, M.; Xu, S. T.; Chen, H. J.; Zhang, C. F.; Xu, J., *Green Chem* **2014,** *16* (5), 2523-2527.
15. (a) Hu, Z.; Kerton, F. M., *Organic & Biomolecular Chemistry* **2011,** *10* (8), 1618-1624; (b) Huang, B.; Tian, H.; Lin, S.; Xie, M.; Yu, X.; Xu, Q., *Tetrahedron Lett* **2013,** *54* (22), 2861-2864.
16. (a) Zhu, B.; Lazar, M.; Trewyn, B. G.; Angelici, R. J., *Journal of Catalysis* **2008,** *260* (1), 1-6; (b) Patil, R. D.; Adimurthy, S., *Advanced Synthesis & Catalysis* **2011,** *353* (10), 1695-1700.
17. Prades, A.; Peris, E.; Albrecht, M., *Organometallics* **2011,** *30* (5), 1162-1167.
18. He, L. P.; Chen, T.; Gong, D. R.; Lai, Z. P.; Huang, K. W., *Organometallics* **2012,** *31* (14), 5208-5211.
19. Stubbs, J. M.; Hazlehurst, R. J.; Boyle, P. D.; Blacquiere, J. M., *Organometallics* **2017,** *36* (9), 1692-1698.

20. (a) Magyar, A.; Hell, Z., *Monatsh Chem* **2016,** *147* (9), 1583-1589; 1
(b) Liu, H. H.; Chuah, G. K.; Jaenicke, S., *Journal of Catalysis* **2015,** *329*,
262-268.

21. Landge, S. M.; Atanassova, V.; Thimmaiah, M.; Torok, B.,
Tetrahedron Letters **2007,** *48* (29), 5161-5164.

22. (a) Bellows, S. M.; Chakraborty, S.; Gary, J. B.; Jones, W. D.;
Cundari, T. R., *Inorg Chem* **2017,** *56* (10), 5519-5524; (b)
Gnanaprakasam, B.; Zhang, J.; Milstein, D., *Angew Chem Int Edit*
2010, *49* (8), 1468-1471; (c) Zeng, G.; Sakaki, S.; Fujita, K.-i.; Sano, H.;
Yamaguchi, R., *ACS Catalysis* **2014,** *4* (3), 1010-1020.

23. Cavani, F.; Trifiro, F.; Vaccari, A., *Catalysis Today* **1991,** *11* (2),
173-301.

24. Meloni, D.; Sini, M. F.; Cutrufello, M. G.; Monaci, R.; Rombi, E.;
Ferino, I., *Journal of Thermal Analysis and Calorimetry* **2011,** *108* (2),
783-791.

25. Scavetta, E.; Berrettoni, M.; Giorgetti, M.; Tonelli, D.,
Electrochimica Acta **2002,** *47* (15), 2451-2461.

26. Bert, F. S.; Dirk, E. D. V.; Pierre, A. J., *Catalysis Reviews* **2001,** *43*
(4), 443488.

27. Motokura, K.; Hashimoto, N.; Hara, T.; Mitsudome, T.; Mizugaki,
T.; Jitsukawa, K.; Kaneda, K., *Green Chem* **2011,** *13* (9), 2416-2422.

28. Motokura, K.; Nishimura, D.; Mori, K.; Mizugaki, T.; Ebitani, K.;
Kaneda, K., *J Am Chem Soc* **2004,** *126* (18), 5662-5663.

29. Bain, J.; Munro, C. M.; Cho, P.; Voutchkova-Kostal, A. M., *New
Journal of Chemistry* **2012,** *In preparation*.

30. (a) Choudary, B. M.; Madhi, S.; Chowdari, N. S.; Kantam, M. L.;
Sreedhar, B., *Journal of the American Chemical Society* **2002,** *124*
(47), 14127-14136; (b) Bain, J.; Cho, P.; Voutchkova-Kostal, A., *Green
Chemistry* **2015,** *17* (4), 2271-2280; (c) Wu, Z. Y.; Zhu, Q. Q.; Shen, C.;
Tan, T. W., *Acs Omega* **2016,** *1* (4), 498-506.

31. Fang, W. H.; Zhang, Q. H.; Chen, J.; Deng, W. P.; Wang, Y., *Chem
Commun* **2010,** *46* (9), 1547-1549.

32. Mitsudome, T.; Mikami, Y.; Ebata, K.; Mizugaki, T.; Jitsukawa, K.;
Kaneda, K., *Chem Commun* **2008,** (39), 4804-4806.

33. Bennur, T. H.; Ramani, A.; Bal, R.; Chanda, B. M.; Sivasanker, S.,
Catal Commun **2002,** *3* (10), 493-496.

34. Naresh, D.; Kumar, V. P.; Harisekhar, M.; Nagaraju, N.;
Putrakumar, B.; Chary, K. V. R., *Appl Surf Sci* **2014,** *314*, 199-207.

35. Yaseneva, P.; An, N.; Finn, M.; Tiedemann, N.; Voutchkova-
Kostal, A.; A., L., *Chem. Materials, In Review* **2017**.

36. Sing, K. S. W., *Pure Appl Chem* **1982,** *54* (11), 2201-2218.

37. Pérez-Ramírez, J.; Mul, G.; Moulijn, J. A., *Vibrational
Spectroscopy* **2001,** *27* (1), 75-88.

38. Moulder, J. F.; Chastain, J.; King, R. C., *Handbook of x-ray
photoelectron spectroscopy : a reference book of standard spectra
for identification and interpretation of XPS data*. Physical Electronics:
Eden Prairie, Minn., 1995; p 261 p.

39. (a) Yamaguchi, R.; Ikeda, C.; Takahashi, Y.; Fujita, K., *Journal of
the American Chemical Society* **2009,** *131* (24), 8410-+; (b) Wang, Q.;
Chai, H.; Yu, Z., *Organometallics* **2018,** *37* (4), 584-591; (c) Wu, J. J.;
Talwar, D.; Johnston, S.; Yan, M.; Xiao, J. L., *Angew Chem Int Edit*
2013, *52* (27), 6983-6987.

40. Hale, L. V. A.; Malakar, T.; Tseng, K. N. T.; Zimmerman, P. M.; Paul,
A.; Szymczak, N. K., *Acs Catalysis* **2016,** *6* (8), 4799-4813.

41. Lamblin, M.; Nassar-Hardy, L.; Hierso, J. C.; Fouquet, E.; Felpin, F.
X., *Advanced Synthesis & Catalysis* **2010,** *352* (1), 33-79.

42. (a) Richardson, J. M.; Jones, C. W., *Advanced Synthesis &
Catalysis* **2006,** *348* (10-11), 1207-1216; (b) Richardson, J. M.; Jones,
C. W., *Journal of Catalysis* **2007,** *251* (1), 80-93.

43. Lee, A. F.; Ellis, P. J.; Fairlamb, I. J. S.; Wilson, K., *Dalton
Transactions* **2010,** *39* (43), 10473-10482.